UV femtosecond laser photochemistry of TNT: A near field scanning optical microscopy study

UV FEMTOSECOND LASER PHOTOCHEMISTRY OF TNT: A Near Field Scanning Optical Microscopy Study

By

Lewis Mortimer Gomez De Arco

A thesis submitted in partial fulfillment of the requirements for the degree of

MASTER OF SCIENCES
in
CHEMISTRY

UNIVERSITY OF PUERTO RICO
MAYAGÜEZ CAMPUS
2004

Approved by:

_____	_____
Julio Briano, PhD Member, Graduate Committee	Date
_____	_____
Samuel Hernandez, Ph.D. Member, Graduate Committee	Date
_____	_____
Miguel Castro, Ph.D. President, Graduate Committee	Date
_____	_____
Jose Colucci, PhD. Representative of Graduate Studies	Date
_____	_____
María A. Aponte, Ph.D Chairperson of the Department	Date

ABSTRACT

Laser-based sensor development has become a field of interest due to environmental and security reasons. In this work, an ultrafast femtosecond pulsed laser was coupled to an AFM/NSOM system to study the photochemistry of particles and solutions of TNT under environmental conditions. Vibrational spectroscopy analysis performed on the dry deposits of irradiated TNT solutions reveals that photolysis products of TNT solutions depend on the solvent nature. Nanosized TNT particles were deposited on a transmissive substrate and characterized by atomic force and electron microscopy. The chemical composition of the particles was confirmed by surface reflection FTIR and energy dispersive X-ray spectroscopy analysis. TNT single particles showed fluorescence signal upon illumination with 266 nm pulses within the near field. The fluorescence signal is attributed to photo-dissociated NO due to TNT fragmentation, and the fluorescence yield resulted to be characteristic of a multi-photon absorption process. These results represent a significant advance in the chemical trace detection of warfare agents in open environments.

RESUMEN

El desarrollo de sensores basados en tecnología láser se ha convertido en un campo de gran interés debido a razones medioambientales y de seguridad. En este trabajo se acoplo un sistema láser de pulsos ultrarrápidos de femtosegundos a un sistema AFM/NSOM para estudiar la fotoquímica de soluciones y partículas de 2,4,6-Trinitrotolueno (TNT). El análisis de espectroscopia vibracional sobre depósitos de soluciones de TNT, que habían sido irradiadas previamente con fotones de 266 nm, revelan que los productos de la fotolisis dependen de la naturaleza del solvente. Las partículas de TNT fueron depositadas sobre substratos transparentes y caracterizadas microscópica y espectroscópicamente. Cristales sencillos de este compuesto exhibieron fluorescencia al ser irradiados con pulsos de 266 nm en el campo cercano. La señal de fluorescencia se atribuye a NO foto-disociado debido a la fragmentación de TNT, y su rendimiento resulto ser característico de un proceso de absorción multifotónico. Los resultados obtenidos constituyen un avance significativo en la detección química de trazas de TNT en condiciones abiertas.

ACKNOWLEDGMENTS

First, let’s thank God, my rock and fortress; Who gave me the strength and health to conduct this work. Thanks to my family for their support and sacrifice, for giving me lively example of unconditional love.

For the entire group of sensor development: Each one of you has part in this work, I enjoyed every time I could interact with you all. You definitely gave me good ideas and support. Now, let’s give a good hand to my advisor, Miguel Castro, always mysterious and forgetful, but always very certain. In the few instances where he could actually break his silence, it was just perfect. For all my lab partners, I could say a lot of things to summarize my experience with you in the lab, but sometimes less is better: Thanks.

To my lovely Liliana: You made my stay in Puerto Rico a lot easier; thanks for being my sweetheart, source of my inspiration. I love you.

For all the forgotten ones: Thanks, you know who you are.

CONTENT

1. INTRODUCTION

In recent years, identification and quantification of traces of powerful explosives has constituted an emerging and important topic of interest due to their relevant role in many areas concerning the security and the health of the population. Recent books and extensive reviews confirm this observation [Yinon 2002; Jimenez and Navas 2004]. It has been well established that in field detection and deactivation of hidden weapons, such as buried landmines, it is better to trace the chemical signature of explosives contained in the mines rather than tracing the mine cases [Fisher et al. 2000; Sylvia et al. 2000; Jenkins et al. 2001]. Currently, deminers most frequently use metal detectors and probes to locate landmines, but modern mines have little metal content, limiting severely the use of metal detectors. Probing is extremely dangerous and time consuming. It involves "feeling" mines by methodically inserting rigid rods into the soil. When a solid object is encountered, it is excavated to determine if the object correspond to a mine. Canines have also been used but they do not perform well in all environments. Besides, dog's desire to work and health are critical and poorly controlled variables in the detection process [Nolan et al. 1977]. More technically advanced equipment such as infrared and ground penetrating radars have been developed but they are in their early developing stages. A single solution to this problem does not exist, though chemical tracing of signature compounds in mines arises as a promising high-sensitive method, to decrease the number of false positives in mine detection.

Nearly 80% of the types of mines manufactured worldwide contain 2,4,6-trinitrotoluene (TNT) or mixtures of explosives containing TNT. The mass of TNT contained in these mines ranges from as little as 7 grams to 13 kilograms [Colling 1999]. This mass of TNT is adequate to produce vapors of signature compounds that can be released into the soil for decades. Also, a number of studies of the environmental fate of explosive chemicals in landmines and their transport through

the soil indicate that a detectable amount of explosives reach the surface soil. TNT, its manufacturing impurities and its decomposition products all permeate through the plastic landmine components as well as cracks or pores in the mine casing and migrate to the surface [George et al. 1999; Silvya et al. 2000]. Once out they rapidly absorb on soil solids, due principally to the large surface area of soil particles and to the affinity of explosives to adsorb on solid particles [Kenna et al. 1986]. Some of the common compounds, which are significantly contributors to the chemical fingerprint of the buried landmines, are shown in figure 1.

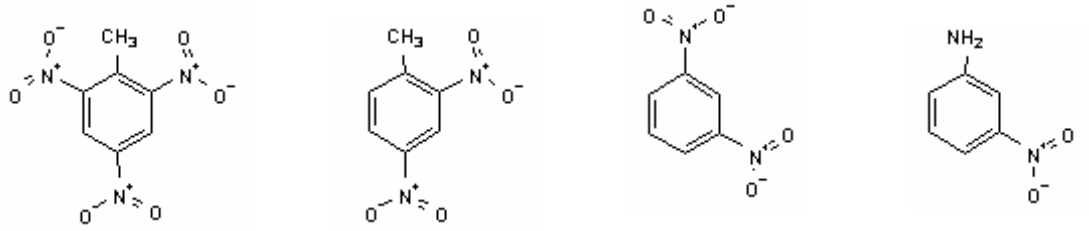

Figure 1. *Chemical structure of important landmine chemical signature compounds. Fisher et al. 2000*

These signature compounds are released into the surrounding soil through surface contamination of landmine cases, by vapor phase diffusion of analyte through the mine structural materials, and by leakage through cracks, seams and holes in the mines [Fisher et al. 2000; Silvya et al. 2000]. The latter two are the primary long-term release mechanisms and only a small fraction will eventually reach the surface of the soil. Thus, the releasing of only trace quantity of explosives from a buried landmine to the environment is expected. Therefore, the use of high sensitivity analytical detection is also required for landmine-explosives field detection.

It is known that TNT, as a nitroaromatic compound, undergoes photo dissociation upon exposure to ultraviolet radiation, resulting in the formation of photodecomposition products [Yinon 1999]. The possible photo dissociation pathways of the simplest nitroaromatic, $C_6H_5NO_2$, are:

$C_6H_5NO_2$	→	$C_6H_5 + NO_2$	reaction 1
$C_6H_5NO_2$	→	$C_6H_5NO + O$	reaction 2
$C_6H_5NO_2$	→	$C_6H_5O + NO$	reaction 3
$C_6H_5NO_2$	→	$C_5H_5 + CO + NO$	reaction 4

Nitric oxide (NO) is one of the principal decomposition products that results from the photodissociation of nitroaromatics; therefore detection of the latter may indicate the presence of the former. NO probing methods that are extensively applied for detection include laser-induced fluorescence (LIF) and Femtosecond, picosecond or nanosecond resonantly enhanced multiphoton ionization (REMPI). REMPI achieves very high sensitivity, whereas LIF achieves less but has the advantage of remote sensing capabilities. The main disadvantage of LIF is the noise that accompanies the signal due to the background at excitation and longer wavelengths. The solutions to overcome background fluorescence include, among others, two-photon excitation [Shu 2000]. Nitroaromatic detection by LIF includes a previous stage of photofragmentation (PF) as shown in figure 2.

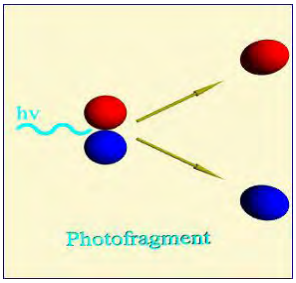

Figure 2. *Illustration of the photofragmentation process for a single molecule. The incident radiation transfers enough energy to the molecule to break a chemical bond.*

The PF/LIF method is particularly suited for the detection of these compounds for they are easily photofragmented in the ultraviolet to generate copious amounts of NO, which can be detected by LIF because it presents strong, well resolved spectral features in the ultraviolet. The photochemical steps involved in the process are described below [Swayambunathan et al. 2000].

$$R\text{-}NO_2 + 2h\nu_1 \longrightarrow R + NO(X^2\Pi) + O \quad \text{(Step 1)}$$
$$NO(X^2\Pi) + h\nu_2 \longrightarrow NO(A^2\Sigma^+) \quad \text{(Step 2)}$$
$$NO(A^2\Sigma^+) \longrightarrow NO(X^2\Pi) + h\nu_3 \quad \text{(Step 3)}$$

Step 1 shows the fragmentation of the nitrocompound to form NO in its ground electronic state, steps 2 and 3 indicate the excitation and ulterior relaxation via fluorescence emission, respectively. Photofragmentation in step 1 can also result in the formation of excited NO, in which case the method is referred as laser photofragmentation/prompt emission spectroscopy. Also, the photons in steps 2 and 3 can be of the same or different frequency, may be time delayed with respect to one another, and may come from the same or different laser [Lemire et al. 1993; Wu et al. 1996; Swayambunathan et al. 2000;].

TNT photochemistry has been widely studied and employed to trace this highly energetic compound by fluorescence detection of its NO photo fragments. Systems that include one or two lasers of equal or different color, with a number of different configurations have been used. Limits of detection that reach the ppb scale have also been reported. However, these photochemical processes have been performed under enclosure and high controlled conditions [Wu et al. 1996; Lee et al. 1997; Shu et al. 2000; Simeonsson et al. 1999; Lopez-Martens et al. 1999; Swayambunathan et al. 2000].

Near-field scanning optical microscopy (NSOM) has attracted much attention in the detection of trace amounts of compounds because it enables microscopy and spectroscopy analysis of localized structures on a nanometer scale [Xie et al. 1994; Trautman et al. 1994, 1996]. This technique involves a nanosized light source, frequently much smaller than the optical wavelength, which is scanned within the near field of the surface of a sample. It has been successfully utilized to study a wide variety of samples that range from solid nano-devices to single molecules [Betzig and Hichester 1993; Hess et al. 1994; Xie and Dunn 1994; Trautman et al 1994; Dunn

1999]. A well known effect is the substantial field enhancement near the tip extremity while illuminating with NSOM. Reports of near field enhancement of confined electric field have demonstrated this fact theoretically and experimentally, giving rise to several nonlinear phenomena such as second harmonic generation and background fluorescence from the tip itself [Dunn 1999; Bouhelier et al. 2004]. The unique characteristics of NSOM make it an appropriate tool to obtain, in the same analysis, correlated topographical and photochemical information from a heterogeneous sample with nanoscale resolution. Therefore, it can be projected as a promising method to detect very small traces of signature landmine compounds, which are known, to be very sensitive to light irradiation.

1.1 Research objective and thesis outline.

The main objective of this project is to implement the application of near field scanning optical microscopy to the study of the photochemistry of trace quantities of high power explosives, in order to enable their detection. The photochemical properties of these materials have been used previously to trace them, but only a few attempts had been made on this topic on open environments. The second focus of this thesis is to study the photochemistry of TNT solutions upon irradiation with UV ultrashort pulses in different environments. This is important to establish if there is a direct participation of the media surrounding the TNT molecules in their final photodecomposition products.

This thesis is structured in six (6) main chapters and is organized as follows: The theoretical background on photochemistry and near field scanning optical microscopy is presented in chapter 2. In chapter 3, a detailed description of the previous work that have been found in the literature concerning this research main topics is presented. A detailed and complete description of the methods and apparatus systems used for this research will be found in chapter 4; we will show how a pulsed femtosecond laser has

been combined to an aperture NSOM system to induce photochemical processes within the near field. In chapter 5 the experimental results are presented and extensively discussed, comparing them with what is known currently in the field. Chapter 6 outlines the general conclusions and possible areas of future work.

2. THEORY

2.1 Photochemistry

Photochemistry is the name used to group the number of chemical processes that are brought about from matter–light interaction. Photochemical reactions in laboratory environments have been known for almost as long as Chemistry has been studied. Most of the observations were accidental and remained uninterpreted, and only at the end of nineteenth century any systematic approach was made. Today, photochemistry applications range from the synthesis of new and complex organic species through numerous kinds of images and photographic process, to the advantage and storage of solar energy. The significance of photochemistry involves chemistry at its most fundamental level. The reactions, dissociations, isomerizations, and optical absorption and emission of electronically excited species are the central future of this field.

2.2 Photochemical processes

Photochemical processes involving the absorption of light can be divided into absorption and the subsequent fate of the electronically excited species formed. Figure 3 summarizes the most important processes by which an electronic excited species may lose its energy; each will be defined below [Wayne 1988].

2.2.1 Dissociation: The process whereby the excited state species is split into simpler fragments which may be smaller molecules, atoms, ions or free radicals. Reactions of this type are important in gas phase and atmospheric chemistry. Many species can be induced to photodissociate:

$[X\text{-}Y]^{*} \longrightarrow X + Y$

$[Cl\text{-}Cl]^{*} \longrightarrow Cl^{\cdot} + Cl^{\cdot}$

$[NO_2]^{*} \longrightarrow NO + O$

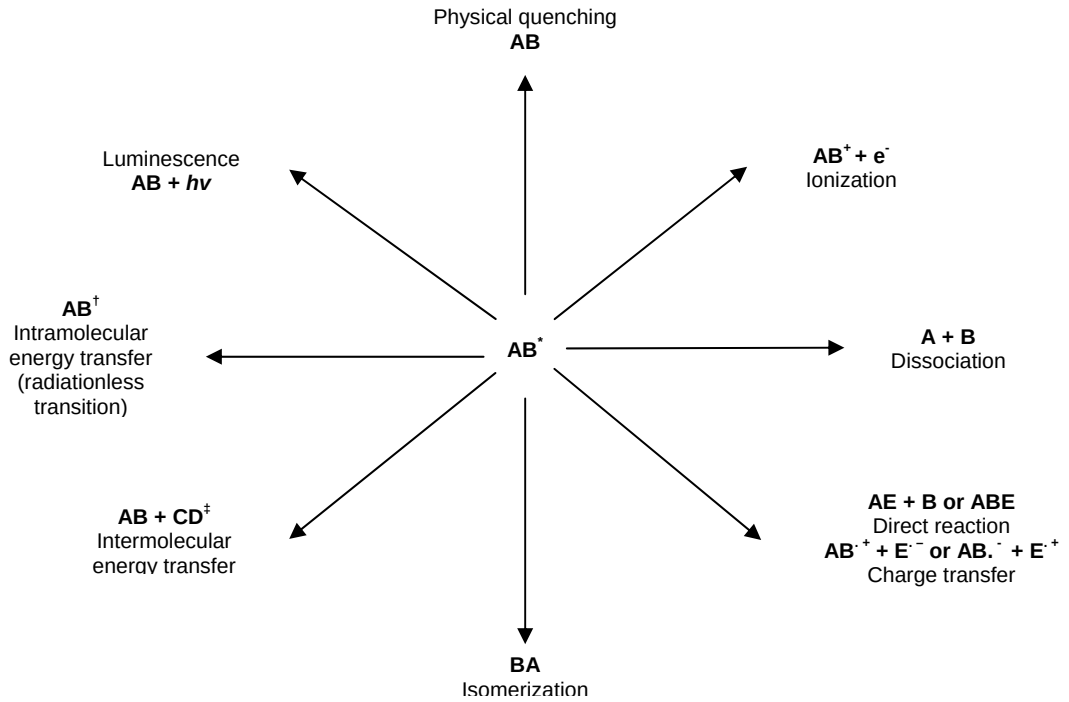

Figure 3. *The several routes to loss of electronic excitation. The use of symbols *, † and ‡ illustrate the presence of electronic excitation and not necessarily differences in states. Wayne 1988*

2.2.2 Direct Reaction: The photoexcited state may also undergo reactions that are definitively unavailable to the ground state species. For example, a photoexcited ketone can undergo a 2+2 cycloaddition with an alkene to give an oxetane (a cyclic ether with a four membered ring).

$[X\text{-}Y]^{*} \xrightarrow{+z} XYZ$

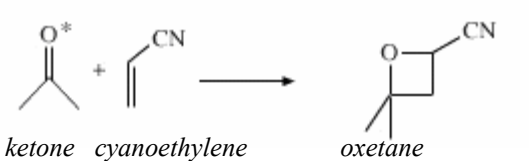

ketone *cyanoethylene* *oxetane*

2.2.3 Isomerization: Photoexcited species may convert into an isomer. For example, *trans*-stilbene can be photoexcited to a state that allows free rotation around the alkene's double bond. The photoexcited species is able to relax back to the ground state at any time, and if this happens when the excited stilbene is in the *cis* conformation, ground state *cis*-stilbene will be formed.

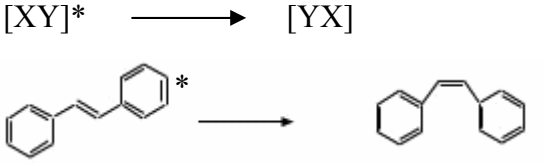

trans-stilbene *cis*-stilbebe

2.2.4 Intermolecular energy transfer: An excited state species can transfer energy to another that is in its ground state. This process is commonly used to produce singlet oxygen. A molecule is photoexcited with UV light. The photoexcited species is able to transfer energy to triplet oxygen, which is converted to singlet oxygen.

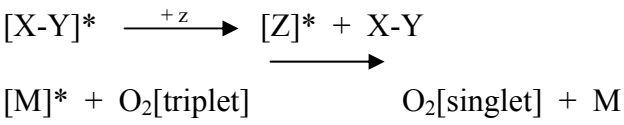

2.2.5 Intramolecular energy transfer: The excited state may undergo intersystem crossing and relax in an intramolecular manner. For example, the S1 (excited singlet) state of naphthalene can convert into the T1 (excited triplet) state.

$$[X\text{-}Y]^* \longrightarrow [X\text{-}Y]^\dagger$$

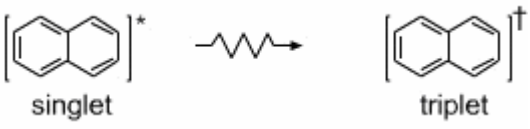

2.2.6 Luminescence: When molecules absorb UV and visible radiation they undergo either electronic or simultaneous electronic and vibrational excitation. Some of the absorbed energy is given off as heat to the solvent, and some is emitted as radiation. In some unique chemical reactions radiation is emitted while a reaction is occurring. In general, the emitted radiation in these processes is called *luminescence*.

$$[X\text{-}Y]^* \longrightarrow X\text{-}Y + h\nu$$

$$Na^* \longrightarrow Na + h\nu$$

Specific luminescence phenomena such as *fluorescence*, *phosphorescence*, and *chemiluminescence* form the basis of some very sensitive analytical methods.

Excitation of an electron (σ-bonding, π-bonding, or non-bonding in organic molecules) in the highest occupied molecular orbital (HOMO) of the electronic ground state S_0, to an unoccupied molecular orbital creates an excited electronic state, S* (e.g., S_1 or S_2). In the excited singlet state, the spin of the excited electron remains paired with the electron left behind in the ground state HOMO. The electronic excitation is often accompanied by a simultaneous change in the vibrational energy of the molecule. From the electronic-vibrational excited state, relaxation to the lowest vibrational level occurs by a radiationless process. This is followed by fluorescence, which is the relaxation to the electronic ground state by emission of radiation.

From the excited singlet state, crossover to a vibrationally excited triplet state (intersystem crossing) can also occur. In the triplet state, the spin orientation of the

excited electron has flipped, so that the spins of the original electron pair are now parallel. The emission of radiation due to relaxation from a triplet to singlet state is known as phosphorescence. Since triplet to singlet transitions are much less probable than singlet to singlet transition, phosphorescence is a much slower process than fluorescence.

Chemiluminescence is the emission of radiation during a chemical reaction. An example is the oxidation of luminol by hydrogen peroxide in an alkaline solution catalyzed by a metal ion. Very low concentrations of metal ions can be determined using this method.

2.2.7 Quenching: In the liquid state, the excited state species may be quenched in which the energy of the excited state species is converted into vibrational energy (heat).

$$[X\text{-}Y]^* \xrightarrow{m} X\text{-}Y + m^* \qquad \text{Where: m = solvent}$$

2.2.8 Ionization: Photoionization processes are of great importance high in the atmosphere where pressures are low and short wavelength UV radiation from the sun has a high flux. It is widely used as a powerful tool in the development of detection methods of compounds, aided by the use of laser based techniques.

$$[X\text{-}Y]^* \longrightarrow [X\text{-}Y]^{\cdot +} + e^-$$

$$NO + h\nu_{[134,3nm]} \longrightarrow [NO]^* + e^-$$

2.2.9 Secondary reactions

The products that result from these photochemical processes can themselves participate in chemical reactions which are a direct consequence of the initial absorption of a quantum of radiation. These reactions are commonly called *secondary* reactions because they are direct consequence of the *primary* photophysical processes. For example, consider the photolysis of ketene:

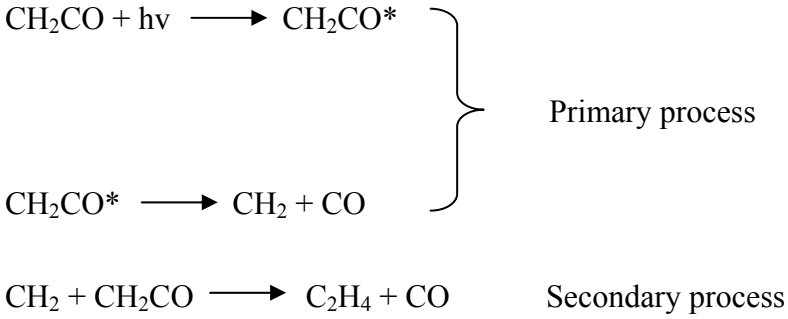

Most common intermediates include free atoms and radicals, as well as electronically excited species. Such entities are frequently highly reactive, with a consequently short lifetime in the reaction. Chain reactions are typical of atoms and free radicals, and such processes are frequently encountered in photochemistry.

An important concept in photochemistry is that of ***quantum yield***, that is the number of molecules of reactant consumed for each photon of light absorbed. In some cases a distinction is made between a primary quantum yield φ for a specific primary process and an overall quantum yield Φ for the complete system of reactions, if present.

2.3 Photochemistry of Nitroaromatics

Nitroaromatic compounds strongly interact with UV-Vis radiation leading to a number of different possible reactions. Here, examples of the principal photochemical processes that may occur are presented.

2.3.1 Dissociation into free radicals

Nitroaromatics dissociate upon ultraviolet irradiation to release NO_2 with further dissociation to NO. However, it can react with the phenyl radical for a global rearrangement process.

$$C_6H_5\text{-}NO_2 \xrightarrow{h\nu} C_6H_5^{\cdot} + NO_2 \longrightarrow C_6H_5O^{\cdot} + NO \longrightarrow C_6H_5ONO$$

2.3.2 N-O bond rupture

It is well recognized that NO_2 dissociates efficiently to NO and O with $\varphi = 0.97$. The energy of dissociation for this process is approximately 72 kcal/mol.

$$C_6H_5\text{-}NO_2 \xrightarrow{h\nu} C_6H_5\text{-}N{=}O + O$$

It has been reported that nitrobenzene dissolved in benzene, a hydrogen deficient solvent, is stable when irradiated with 366 nm photons.

2.3.3 Hydrogen abstraction

This type of process is characteristic of molecules with close n, π^* excited states.

$$C_6H_5NO_2 \xrightarrow{h\nu} C_6H_5NO_2^{*} \xrightarrow{R'\text{-}H} C_6H_5NO_2H + R'^{\cdot}$$

Nitroaromatics also work as photooxidants. The formation of aniline has been demonstrated and all of the intermediate products of reduction from irradiation of nitrobenzene in alcohols [Albini and Fagnoni 2004]. Evidence has been found for the formation of p-aminophenol due to photoreduction of nitrobenzene dissolved in methanol. Hydrogen abstraction from the solvent is the principal mechanism by which this reaction is brought. Nitrobenzene first is transformed into phenyl hydroxylamine and then, rearranged to the final product.

2.3.4 Light catalyzed rearrangements

In general, most aromatics with hydrogen ortho to a nitro group will be sensitive to light. NO_2 is reduced to NO and the O atom is inserted in the C-H bond to give C-OH.

$$C_6H_5(NO_2)(RR'CH) \xrightarrow{h\nu} C_6H_5(NO)(RR'COH)$$

2.3.5 Photo-induced nucleophylic substitution for nitroaromatics

Several experiments have demonstrated that there is a direct attack to the benzene ring. Nucleophyle nature plays a major role in defining the place of attack.

$$p\text{-}C_6H_5(OCH_3)(NO_2) \xrightarrow{hv,\ CH3NH2} p\text{-}C_6H_5(HNCH_3)(NO_2) + CH_3OH$$

$$p\text{-}C_6H_5(OCH_3)(NO_2) \xrightarrow{hv,\ NaOH} p\text{-}C_6H_5(OH)(NO_2) + p\text{-}C_6H_5(OCH_3)(OH) + CH_3OH + NO_2^-$$

$$p\text{-}C_6H_5(OCH_3)(NO_2) \xrightarrow{hv,\ Pyridine} \text{phenylpyridine} + NO_2^-$$

One example of a characteristic photo-induced nucleophylic attack to the C-NO_2 bond is the irradiation of Trinitrobenzene in basic media

$$\textit{1,3,5}\text{-Trinitrobenzene} \xrightarrow{hv,\ OH-} \textit{3,5}\text{-Trinitrophenol} + NO_2^-$$

2.4 Near Field Scanning Optical Microscopy

2.4.1 History

The first mention of near-field microscopy appeared in the article published by E. Synge in 1928 who suggested a new concept to break the diffraction limit [Synge 1928]. The diffraction limit arises from the size of the spot that a light beam can be focused with normal lenses. The distance, d, from the highest intensity point in the middle of the spot to the first node in intensity is given by:

$$d = 0.61\ (\lambda_0/n \sin\theta) \qquad \text{(Equation 1)}$$

Where λ_0 is the vacuum wavelength, n is the refractive index of the medium in which the light travels and θ is the convergence angle for the focusing element. This equation is usually simplified to $d = \lambda/2$. The maximum resolution achievable is then approximately of 250-350 nm for visible light [Dunn 1999].

In subsequent papers in the 1930s, Synge gives the basis of modern aperture NSOM [Synge 1931, 1932]. Synge proposed forming a microscopic aperture much smaller than the illumination wavelength in an opaque screen. By illuminating the backside of the screen the light passing through the hole would be confined only by the dimensions of the aperture. Once placed in close proximity to the sample surface, the transmitted light could be used to image the surface before it had time to diffract out and degrade the resolution (figure 4) [Dunn 1999; Courjon 2003].

In 1956, O'Kefee attempted an experimental approach by scanning the hole along the illuminated sample, it was possible to detect a super-resolved image with resolution limited only by the hole diameter. Ash and Nicholls described with details a microwave realization allowing sub-wavelength resolution. It was considered as the very first realization of a near-field microscope [O'kefee 1956].

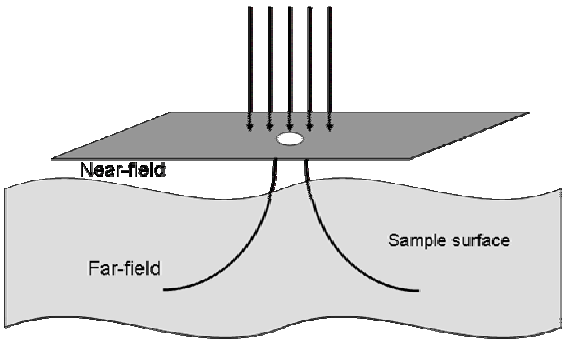

Figure 4. *Schematic of Synge idea for achieving subdiffraction limit spatial resolution. O'kefee 1956*

It was not until 1984 that Pohl's laboratory at IBM Zurich reported subdiffraction-limited optical measurements [Pohl 1984]. The same year, G. Massey using a Fourier approach showed that a resolution of about 30 nm was probably achievable and A. Lewis proposed a super-resolving instrument of 50 nm of resolution [Courjon 2003; Lewis et al. 1984].

2.4.2 NSOM Microscope

One of the common NSOM designs is shown in figure 5. Laser light is passed through a single-mode optical fiber, the end of which is fabricated into the NSOM tip. The near-field tip is mounted on a *z*-piezo tube to control the tip-sample distance during scanning. The sample is mounted on a separate *x*-*y* piezo stage which scans the sample under the tip during the experiment. Light exiting the tip can illuminate or excite fluorescence in the sample. Transmitted or fluorescent emission is collected underneath the sample with a high numerical aperture objective, collected background signal is removed with filters and the sample signal is taken to a photodetector. The software and electronics needed to scan the piezos are similar to those used in atomic force microscopy, then the resulting signal is displayed as intensity versus raster scan position. The topographic image is a normal force map as in conventional AFM [Courjon 2003].

There are some NSOM configurations that can be used; the use of each is often dictated by the sample nature or working environment. The most generally applied NSOM configurations are illustrated in figure 6. In ***transmission mode*** a subdiffraction limited area is illuminated through the probe aperture, transmits through sample and collection occurs with diffraction limited optics. For ***collection mode***, the sample is illuminated with conventional optics and the near-field information is collected by the fiber probe. In the ***illumination/collection mode*** the probe both illuminates the sample and collects the reflected light; it is useful for high scattering and thick samples. Finally, in ***reflection mode*** light source travels through the probe aperture, and reflects from the surface. It presents lower light intensity and is highly tip-dependent, but allows for opaque samples.

Single molecule measurements have demonstrated the sensitivity of NSOM, while the high spatial resolution has revealed undiscovered features in a variety of samples. These two characteristics of NSOM have been amply demonstrated [Dunn 1999; Lewis et al. 2003; La Rosa et al. 1995; Hell et al. 1998; Moerner 1996; Xie 1996; Trautman et al. 1994].

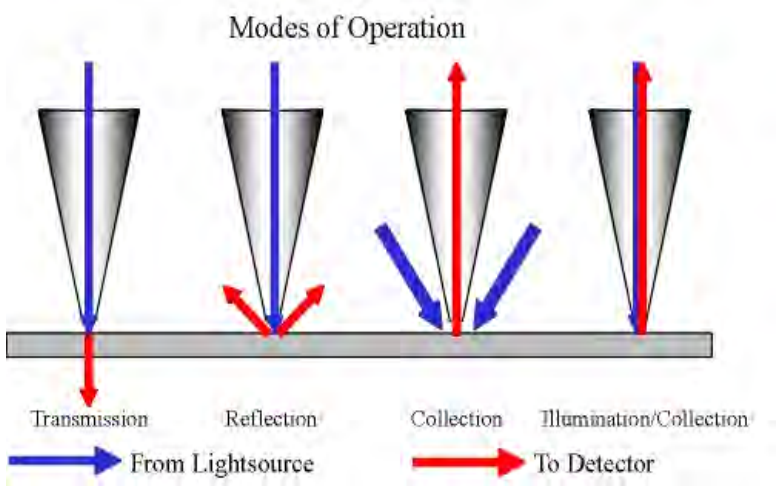

Figure 5. *Schematic of a near-field microscope in the aperture-scanning configuration. Courjon 2003*

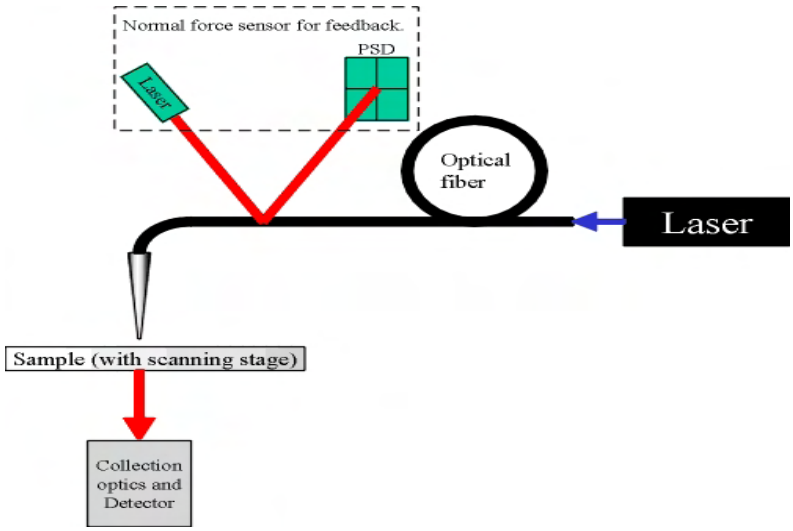

Figure 6*. The typical aperture based NSOM configurations. From left to right: Transmission mode, reflection mode, collection mode and the illumination/collection mode. Dunn 1999*

3. PREVIOUS WORK

The photodegradation of TNT was probably recognized from the earliest days of its manufacture because of the conspicuous color change, to a red or pink, of manufacturing waste waters exposed to sunlight. The most extensive studies of TNT photochemistry were conducted by Burlinson and his co-workers and by Spanggord and his co-workers. Spanggord, in 1980, reported that photodecomposition of TNT was much more rapid in natural sunlight than in darkness. That same year, Burlinson encountered that photo-decomposition was directly proportional to pH over the range 1.1 to 11.1 pH units. At pH 11.1, TNT decomposed even in darkness, possibly as a result of base hydrolysis. Burlinson also attributed the fact that TNT photolysis was more rapid in river water than in distilled water due to the higher pH of the river water, but Spanggord submitted that the effects of pH are insignificant relative to the effects of natural substances in the water. His results indicated that light absorption by substances in natural water sensitizes TNT resulting in photolytic transformations. Similar results were reported by Mabey in 1983. Photolysis has also been reported to be greater in nonpolar than in polar solvents by Suryanarayanan and Capellos 1970, 1972, 1974 [Brannon J.M. and Pennington 2002].

Few studies have reported photolysis products of TNT from natural waters, but Burlinson in 1979 identified an extensive list of products from laboratory irradiation (Appendix 1). He reported that 45 to 50 percent of the photodecomposition products of TNT were recovered in solution with the remainder present as insoluble residues suggestive of oligomers of azo and azoxy compounds, which were not identified. Besides, he proposed that TNT photolysis occurs through 2,4,6-trinitrobenzaldehyde, some undefined nucleophilic complex, and ultimately produces 1,3,5-trinitrobenzene.

This section of previous work will present first the work by Burlinson and collaborators on the identification of TNT photodecomposition products path. Then, it

follows two efforts on tracing TNT with the use of the PF/LIF technique, that take advantage of TNT photochemistry properties to detect it; and a last work that illustrate the use of NSOM fluorescence in single molecule detection.

Burlinson N. E et al. (*1979)* stated that the photolysis of aqueous solutions of 2,4,6-Trinitrotoluene (TNT), at wavelengths of approximately 280 nm, results in initial formation of the 2,4,6-Trinitrobenzyl anion (TNBa). Evidence for this reactive intermediate, photogenerated in acidic or neutral media, is demonstrated by its ability to exchange hydrogen for deuterium in photolized D_2O solutions; among other experiments that will not be covered here.

Previous non-published work by the authors indicated the formation of 2,4,6-Trinitrobenzyl anion from 2,4,6-trinitrotoluene in alkaline tetrahydrofuran-methanol solutions. Bernasconi also found that TNBa is formed as a transient species of upon reaction of TNT with methoxide in methanol, ethoxide in ethanol, or hydroxide in 50% dioxane-water. Also, they have identified ten photodecomposition products in aqueous TNT photolysates (using sunlight or a Pyrex-filtered Hg lamp). The major ones are 2,4,6-trinitrobenzaldehyde, 1,3,5-trinitrobenzene, 2,4,6-trinitrobenzyl alcohol, 4,6-dinitroantrhanil, 2-amino-4,6dinitrobenzoic acid, 2,2'-dicarboxy-3,3',5,5'-tetranitroazobenzene, and 2-carboxy-3,3',5,5'-tetranitro-NNO-azoxybenzene. As can be seen from these products no chemistry occurs at the para nitro position.

D_2O solutions of $4x10^{-4}$ TNT were irradiated for 1h in sunlight at various acidities. Photodecomposition products were analyzed by mass spectrometry.

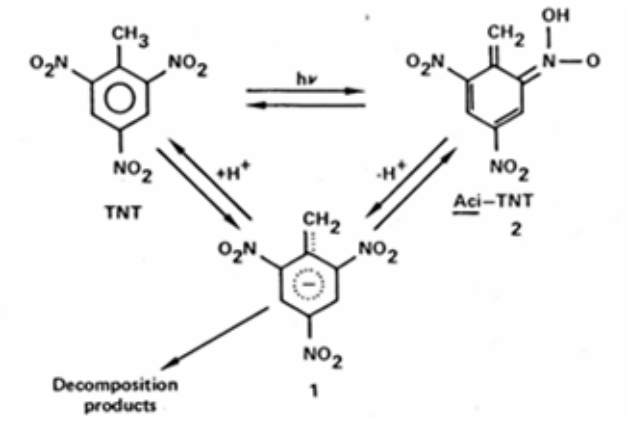

Figure 7. *Proposed mechanism for the formation of 2,4,6-trinitrobenzyl anion due to photolysis of TNT in neutral to acid medium. Burlinson N. E., Sitzman M. E., Kaplan L. A. and Kayser E. Journal of Organic Chemistry, Vol. 44, No. 21, (1979).*

The TNT⟶ 2 ⟶ 1⟶ TNT mechanism for incorporating deuterium into the methyl group of TNT (figure 7) conforms with the observations of Morrison and Migdalof who upon irradiating D_2O/dioxane solutions of *o*-nitrotoluene and *p*-nitrotoluene found deuterium only in the methyl group of *o*-nitrotoluene [Morrison and Migdalof 1965]. The data in table 1 also reveal that as the acidity increases, the decomposition of TNT decreases. This would be in accordance with the scheme showed in figure 7 where a more rapid return of the TNT anion (1) to either TNT or *aci*-TNT (2) would occur as the acidity increase [Burlinson et al. 1979].

Table 1. Photoexchange of 2,4,6-trinitrotoluene in D_2O

pD[a]	10^4 [TNT]$_{60}$[b]	%D[c,d]	% photodecomposition
1.5	**3.31**	**53**	**17.5**
4.0	**2.82**	**47**	**29.6**
7.0	**1.85**	**30**	**53.8**

[a] Adjusted to pD 1.5 and 4.0 with D_2SO_4. [b] [TNT] after 60 minutes. $10^4[TNT]_0 = 4.01$ M. [c] Deuterium assays by NMR of benzene-d6 extracted photolysates. Calculated on the basis of CH_3 ~~CD_3~~ equal to 100% exchange. [d] solutions of TNT in D_2O and/or D_2SO_4 left in the dark for several days showed no deuterium in the TNT. *Burlinson N. E., Sitzman M. E., Kaplan L. A. and Kayser E. Journal of Organic Chemistry, Vol. 44, No. 21, (1979)*

WuD. et al. (1996) performed photofragmentation (PF) of 2,4,6-Trinitrotoluene with subsequent nitric oxide (NO) detection by Laser induced fluorescence (LIF). As TNT luminescence quantum yield is insignificant, it is hard to detect by fluorescence techniques. However, by the use of laser radiation of 226 nm TNT was dissociated to NO_2, the NO_2 rapidly predissociate to produce NO and O. The ground-state NO then absorbs another 226 nm photon to undergo a resonant transition and then produces fluorescence by LIF.

Figure 8 shows the schematic diagram of the experimental set up. A continuous-wave frequency-doubled Nd:YAG laser (532 nm) was used to pump a dye laser. The dye output (622 nm) was mixed together with the continuous-wave frequency-tripled Nd:YAG laser (355 nm) to generate the desired UV laser wavelength (226 nm). The generated laser beam was filtrated and taken to a stainless steel chamber equipped with ultrahigh vacuum components and UV-grade fused silica view ports. The TNT sample, in a stainless steel tube, was connected to the chamber through an on-off valve. The PF-LIF signal was then detected with a photomultiplier tube after being filtered by two long-pass filters. The experiments were conducted in an evacuated cell and under controlled environmental conditions for pure TNT and mixtures of TNT with simulated soil samples.

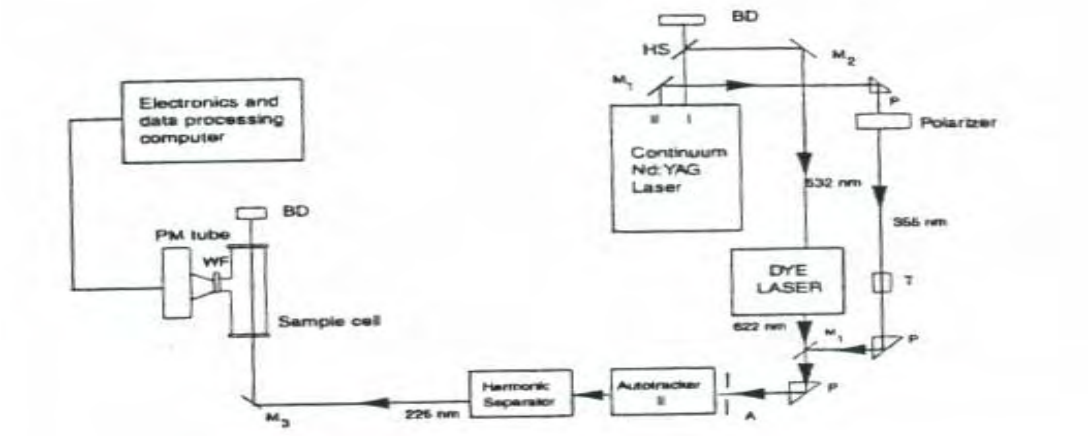

Figure 8. *PF-LIF experimental setup: PM, photomultiplier; BD's, beam dumps; WF, window filter; M3, dichroic mirror (226 nm); HS, harmonic separator; M1's, dichroic mirror (355 nm); M2, dichroic mirror (532 nm); P's, prisms; T, telescope; A, aperture. Dongdong Wu, Jagdish P. Singh, Fang Yueh and David L. Monts. Applied Optics Vol. 35, No. 21 (1996).*

The NO LIF was studied in presence of the buffer gases O_2, N_2 and air at various pressures; where the experimental results demonstrated a larger quenching effect in the LIF signal due to the presence of oxygen. The PF-LIF spectra of pure TNT were recorded at different TNT vapor pressures by varying the temperature. PF-LIF intensity was much higher at high temperature than at room temperature, for which higher temperatures can increase the sensitivity of the PF-LIF technique by increasing the TNT vapor pressure. PF-LIF spectra of TNT were also recorded at different concentrations of TNT in simulated soil. Figure 9 compares two PF-LIF spectra that were recorded at 300 K for pure TNT and a 100 ppm TNT sample. These results showed no significant effect on the main features of the spectra due to these factors; thus, PF-LIF can be used to monitor TNT in soil at high temperatures.

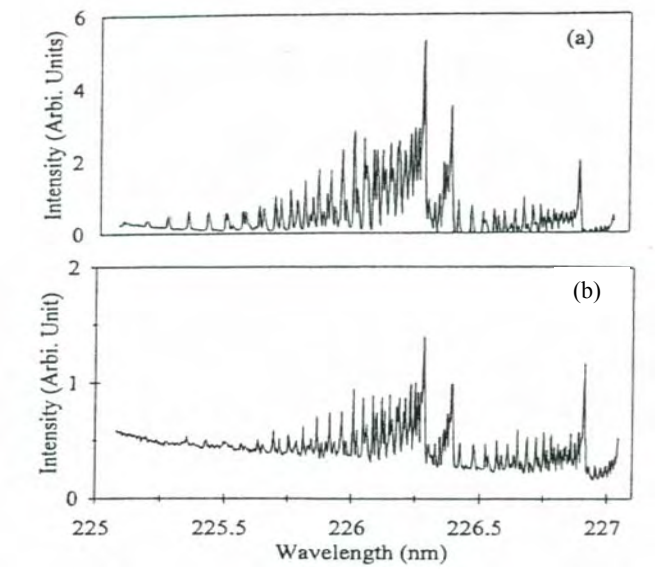

Figure 9 *PF-LIF spectra taken at 300K from a pure TNT sample (a) and from 100 ppm of TNT in soil (b). Dongdong Wu, Jagdish P. Singh, Fang Yueh and David L. Monts. Applied Optics Vol. 35, No. 21 (1996).*

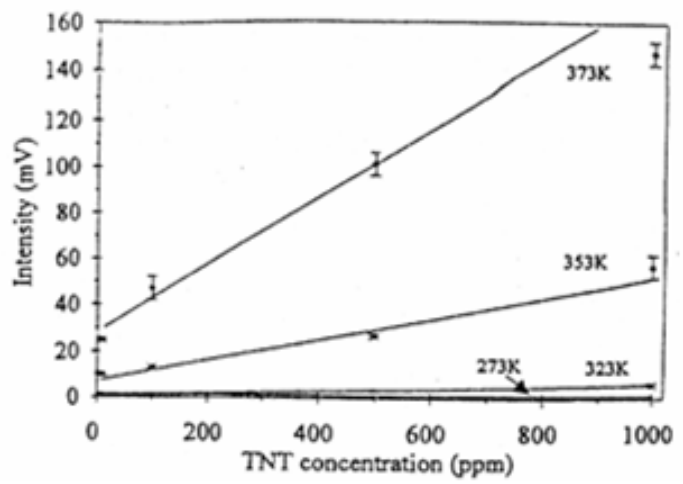

Figure 10. *Illustration of the linear relationship between the intensity of the fluorescence detected by PF-LIF and the initial concentration of TNT at different temperatures. Dongdong Wu, Jagdish P. Singh, Fang Yueh and David L. Monts. Applied Optics Vol. 35, No. 21 (1996).*

Temperature effect on the PF-LIF signal of pure TNT illustrates that the increasing of PF-LIF signal intensity while temperature arises is much faster after 343 K. The TNT concentration calibration curve at different soil temperatures is shown in figure 10. 400 mg of TNT was used for each sample. The detection sensitivity was very poor for sample temperature below 323 K. Signal at high temperature was quite sensitive to heating time of the sample. The limit of detection for TNT in simulated soil was calculated as ~40 ppb. Thus, they demonstrated that PF-LIF holds great promise as a detection technique for TNT in soil [Wu et al. 1996].

Swayambuthan V. et al. (2000), conducted several investigations on the detection of trace concentrations of nitrogen dioxide (NO_2), nitromethane (CH_3NO_2) and 2,4,6-Trinitrotoluene (TNT). Both, one- and two-color laser photofragmentation/fragment detection spectrometry is employed using one or two lasers. PF/LIF is performed using a single laser operating at 227, 355 or 454 nm. They used a 355 nm beam for additional analyte photofragmentation in order to improve the one-color PF/LIF sensitivity.

Figure 11 shows the experimental setup used to conduct one- and two- beam PF/LIF studies on the chosen nitrocompounds. The photolysis cell is a six-arm stainless steel cross of which two opposite arms provide the optical paths for the pump and the probe beams. A third arm, which is normal to the opposing two arms, serves as a viewport for LIF monitoring.

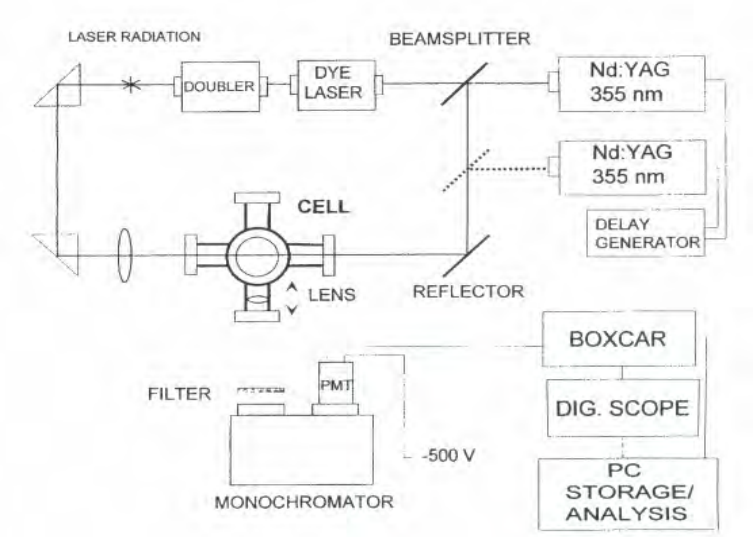

Figure 11. *Diagram of the experimental apparatus used to detect NO fluorescence by the PF-LIF process. Vaidhanat Swayambuthan, Rosario Sausa, and Gurbax Singh. Applied Spectroscopy, 54, 651-658, 2000.*

The fluorescence was collected normal to the laser excitation beam and then focused on a photomultiplier tube. A 250 nm bandpass interference filter (full width at half-maximum of 30 nm) was also used for signal discrimination and to minimize the intensity of scattered light. The excitation spectra was recorded by setting the monocromator at 237 nm and scanning the laser at 0.003 or 0.005 nm/s, whereas the emission spectra was collected by exciting the sample at either 227 or 454 nm and scanning the monocromator at 0.1 nm/s.

NO, NO_2 and nitromethane samples of various concentrations were prepared by dilution with nitrogen. Gas samples flowed by the photolysis cell at a rate of ~ 500 cm^3/min. For TNT, milligrams of TNT were sampled at 1 atm with the use of a miniature oven, ranged from room temperature to 400 K. The output vapors,

photolysis products or both were taken to a pipe with a linear air velocity of ~50 cm/s. For all the measurements, pure compounds, non-evacuated sample cell and controlled environmental conditions were used.

Figure 12(a) shows the emission spectra of NO from NO_2 with and without the 355 nm beam. Similar experiments on NO show nearly the same emission intensity when excited at 227 nm in the presence and absence of the 355 nm beam, no enhancement in the LIF with two colors, which implies that the 355 nm beam from the same Nd:YAG laser is used for additional NO_2 fragmentation. In figure 12(b), observed and calculated PF/LIF emission spectra of NO from NO_2 are presented. Calculated spectrum is generated by using a multiparameter program based on Boltzmann rotational distribution analysis at 300 K. The two spectra are very similar, which implies a photofragmentation/fragment detection process, where NO_2 is fragmented into NO ($X^2\Pi$). The NO fragment in turn is photoexcited, resulting in fluorescence.

The NO_2 PF/LIF signal was measured as function of the pump laser energy at 355 nm. Figure 13(a) shows that the signal increases linearly, doubling at 5 mJ of laser energy, and then plateaus at laser energies above 9 mJ. This result suggests that the step involving photofragmentation of NO_2 to NO might be saturated at higher laser energies. CH_3NO_2 PF/LIF results were very similar to those showed by NO_2 Figure 13(b) shows the linear dependence on laser energy for the 355 nm beam. Also, the signal shows no leveling off as in NO_2 case. The excitation and emission spectra of TNT resulted to be virtually identical from that obtained from NO. This observation clearly suggests a photofragmentation mechanism that involves formation of NO from TNT [Swayambuthan et al. 2000].

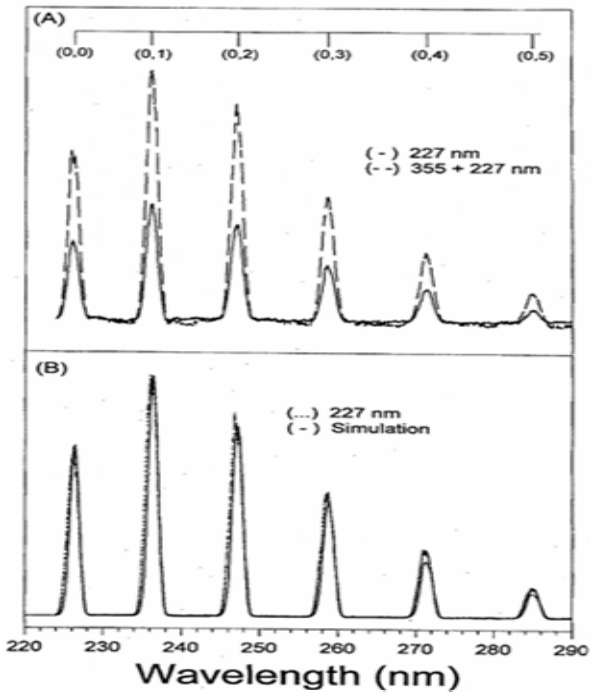

Figure 12. **(A)** Emission spectra of NO from NO_2 at 227 nm (——) and 355 + 227 nm (-----) **(B)** LIF spectra of NO with 227 nm excitation. Experimental (·····) and simulated (——). *Vaidhanat Swayambuthan, Rosario Sausa, and Gurbax Singh. Applied Spectroscopy, 54, 651-658, 2000.*

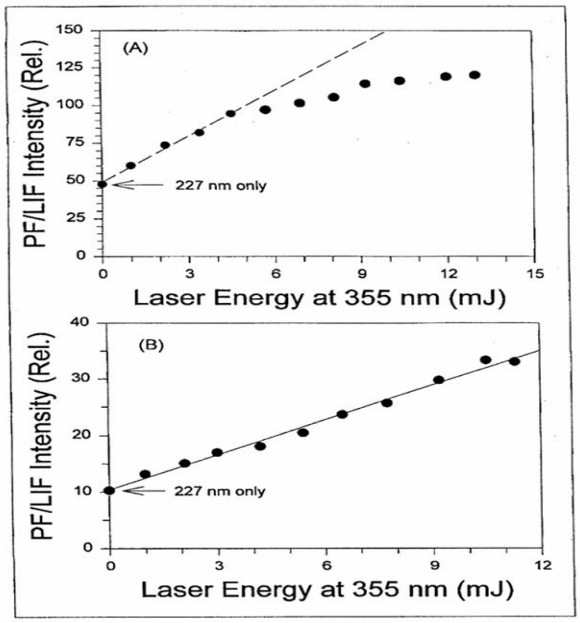

Figure 13. *PF-LIF intensity of NO_2 **(A)** and CH_3NO_2 **(B)** as a function of laser energy at 355 nm. The data error bars are about the same size as the symbols. Vaidhanat Swayambuthan, Rosario Sausa, and Gurbax Singh. Applied Spectroscopy, 54, 651-658, 2000.*

Trautman, J. K. et al. (1994), demonstrated room-temperature emission spectroscopy of single molecules with NSOM. They observed that the emission spectra of single DiI molecules changes with time. The abrupt jumps of the signal are characteristic of single-molecule behavior. Here, the authors show that NSOM can be used to obtain time-dependent emission spectrum of a single molecule in air at room temperature, with a spatial resolution of about 100nm. The spectra of individual molecules exhibit shifts of ±8 nm relative to the average spectrum. The spectra also vary in width by up to 8 nm, some being as broad as the far-field bulk spectrums. The emission spectra of some individual molecules showed time-dependent shifts of up to 10 nm. This variety in spectral position, width, and shape and time dependence can be understood within a model of inhomogeneous broadening in which there is a distribution of barrier heights to rearrangement of the molecular local environment.

An aluminum coated, tapered optical fiber probe with a 100 nm tip aperture, was used to illuminate with 529 nm the surface of a thin film of polymethylmethacrylate (PMMA); on which 1,1'-dioctadecyl-3,3,3',3'-tetra-methyliindocarbocyanine (diI) molecules had been dispersed. Fluorescence was collected through a silica coverslip by an NA 1.4 microscope objective, and detected by either a low-noise avalanche photodiode, or a CCD camera for single-molecule spectroscopy.

In figure 14, the inset shows a near-field fluorescence image of individual diI molecules on PMMA. Single-molecule fluorescence spectra were obtained for the isolated particles. The displayed spectrum B is the average of 21 1-min integrations, and lies near the center of the distribution of fluorescence wavelengths. Spectrum A is the average of 5 1-min integrations, and lies on the high energy side of that distribution, being shifted ~10 nm to the blue.

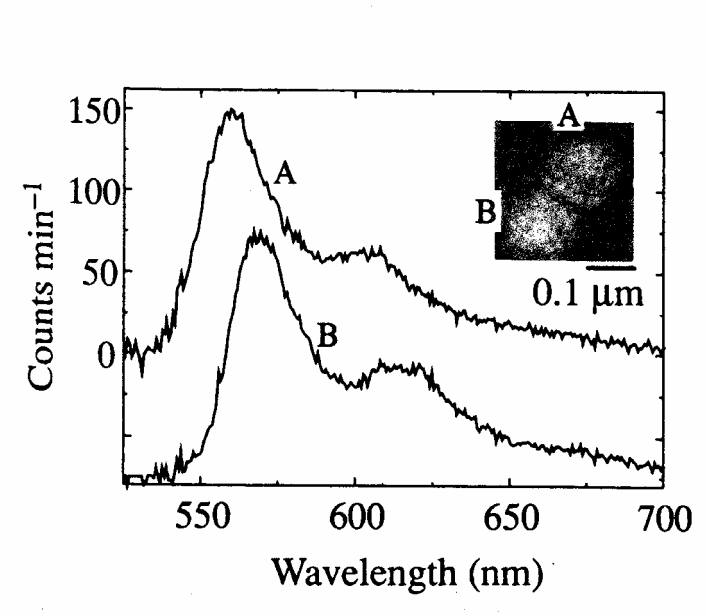

Figure 14 *The near-field fluorescence image of two adjacent molecules A and B (see inset) and the corresponding fluorescence spectrum of each. Trautman, J. K.; Macklin, J. J.; Brus L.E. and Betzing, E. Nature 1994, 369, 40.*

In addition to the spectral variations of wavelengths and widths among molecules, the emission spectra of the individual molecules were observed to vary in time. Figure 15 clearly shows this effect, where after 17 min the spectrum was invariant, it red shifted 5 nm during the eighteen minute and bleached the following minute.

The interpretation of the variability in the spectral width of single molecules is that those molecules that have narrow spectra sit in rigid environments. Those having broader spectra exist in more dynamic surroundings in which molecular reorientation of the matrix molecules, and the concomitant shift in the emission wavelength occurs many times within the 1-min spectral integration. The spectral jumps are also interpreted within this scheme. In this case, changes in the local environment occur in the timescale of minutes rather than seconds. Finally, there was not found any correlation between the various bandshapes and the spectral shift. [Trautman et al. 1994].

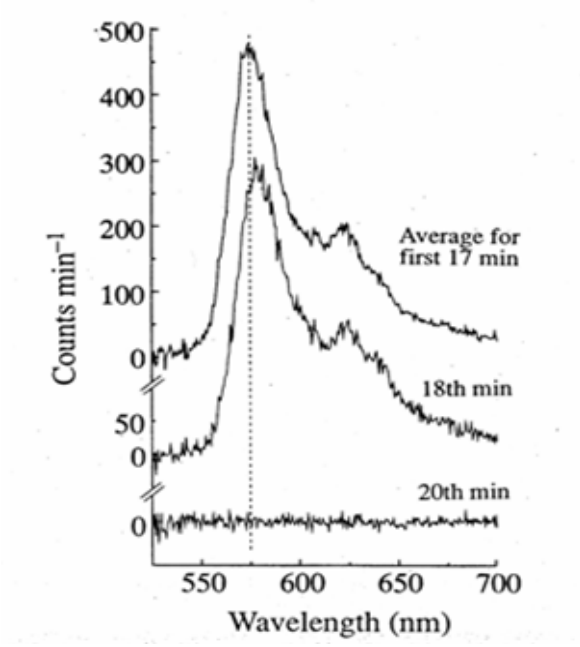

Figure 15. *Single-molecule fluorescence spectra of a highly photostable molecule. Upper trace is the average spectra acquired over 17 min. The trace located in the middle corresponds to the ~5nm shifted spectra acquired in minute 18th. The lowest trace (labeled twentieth minute) correspond to the background. Trautman, J. K.; Macklin, J. J.; Brus L.E. and Betzing, E. Nature 1994, 369, 40.*

4. METHODS

In this section, the different experimental methods employed to study the photochemistry of TNT, whether in solution or as a pure trace, are described. Also, a complete description of the experimental set up employed to combine a commercial fs laser and a near field scanning optical microscopy will be given. The fs laser-NSOM system presented here has been entirely coupled within the framework of this thesis. A schematic approach of the experimental part followed in this work is presented in Figure 16.

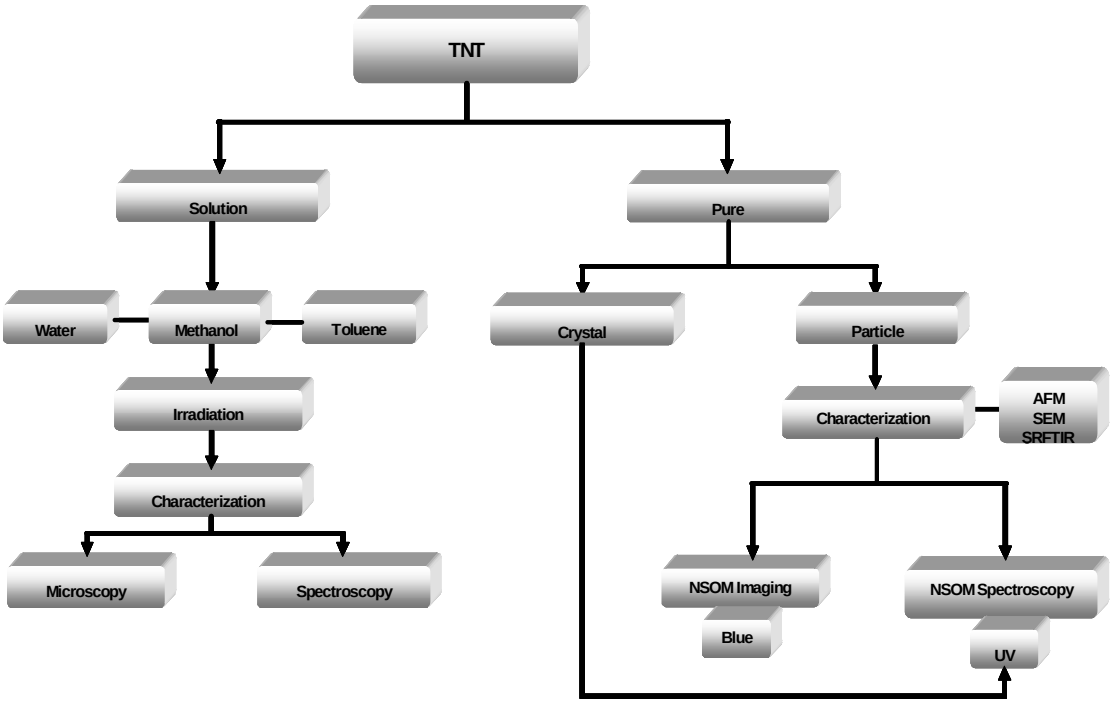

Figure 16. *Schematic representation of the experiments conducted to study the photochemical properties of TNT in solution and as pure trace. TNT solutions in water, methanol and toluene were irradiated and its products characterized using microscopy and spectroscopic techniques. On the other hand, pure solid TNT was used to generate particles, such particles were characterized and used for NSOM imaging and spectroscopy experiments with visible and UV photons. For individual crystalss, only UV photons were employed for NSOM analysis.*

4.1 Description of the set-up

Figure 17 presents an scheme of the complete set up used in this work, in which a *Hurricane* Ti:Saphire laser (Spectra-Physics Lasers) is employed. In this two-laser system, a continuous wave diode-pumped laser pumps a mode-locked Ti:Sapphire laser to generate pulses of 800 mW. Pulses are taken to a regenerative amplifier, in which the pulses are stretched and amplified while interacting with a Nd:YLF laser. After amplified, the pulses are compressed again to generate even shorter pulses of <130 fs of duration, with an energy of approximately 1 mJ. The fundamental radiation is then frequency doubled with the use of a type I phase match crystal to generate 400 nm pulses or frequency tripled by a type I BBO crystal (THG) to generate 266.7 nm pulses.

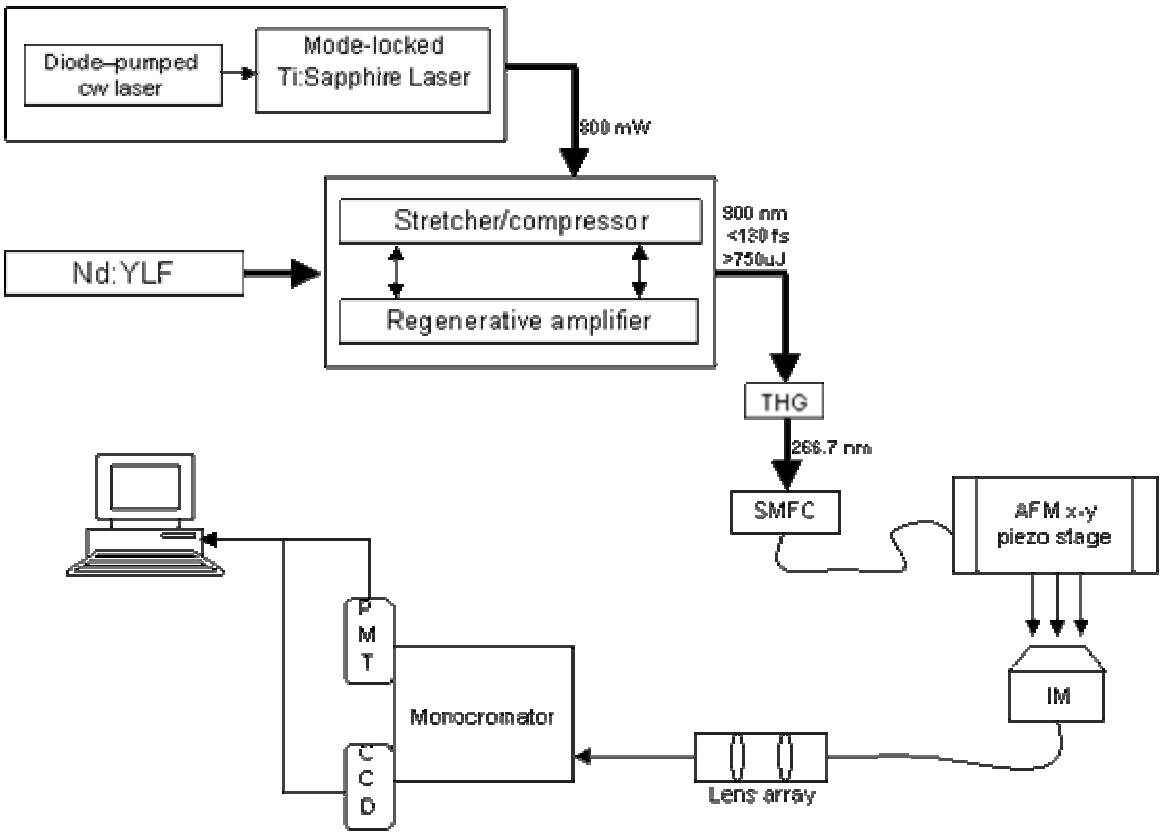

Figure 17 *Schematic of the coupled UV fs laser/Near field scanning optical microscope system used to investigate the NSOM photochemistry of TNT..*

The pulses of interest are coupled to one end of a single-mode optical fiber through a single-mode fiber coupler (SMFC). The other end of the fiber had been pulled to reach a diameter of approximately 250 nm; and covered with an aluminum coating to maximize light throughout. The fiber is attached to an Atomic force microscopy and used as a common AFM tip. Light sent trough the fiber illuminates the sample located on an x-y piezo stage, and the resultant signal is collected with an inverted microscope (IM) equipped with a parabolic-mirror objective and appropriate optics for the wavelengths of interest. Collected signal is focused on a monocromator, and then directed to a photodetector, which could be whether a photomultiplier tube (PMT) or a charged coupled detector (CCD).

4.2 Photochemistry of TNT in solution

2,4,6-Trinitrotoluene – min 30wt% water and 98% purity, was obtained from Chem service. Samples of 0.01 g of solid TNT were weighted and mixed with 1.2 mL of water, methanol and toluene as solvents. The mixtures were placed in a quartz container and exposed to a ~130 fs pulsed laser beam of 266.7 nm at 1000 Hz of repetition rate for 5 minutes. Samples of TNT before exposition and products formed in solution after interaction were deposited in liquid phase onto a first surface gold mirror and the solvent was allowed to vaporize for 8 hours at room temperature.

UV absorption and surface reflection Fourier transform infrared absorption (SRFTIR) measurements were taken for original samples and photodecomposition products obtained with each solvent used.

4.3 Photochemistry of pure traces of TNT

4.3.1 Synthesis of TNT nanoparticles

A more detailed description of this method can be found elsewhere [Mercado et al. 2004]. 500 ppm TNT solutions in HPLC grade methanol solvent were utilized and introduced into an aerosol chamber connected to ultra-high purity nitrogen as a carrier gas. Hot nitrogen current was adapted to the system to heat the aerosol during the path to the substrate surface. The gaseous nitrogen temperature that was set for the carrier gas was 328K. The TNT particles were deposited on a substrate located 5 cm away from the methanol jet. Three shots of 2 seconds each were sufficient to seed the particles on the substrate. Images of the substrate were taken after the exposition to the methanol jet in order to characterize the particles formed using this method. AFM, and SEM analysis were conducted to study the size and morphology of the seeded particles, EDS and SRFTIR revealed their elemental composition and vibrational signature respectively, while NSOM analysis revealed their optical properties.

4.3.2 NSOM photochemistry of TNT particles

The ultrafast pulsed laser was coupled to a near field scanning optical microscopy (NSOM) in order to study the near field photochemistry of TNT particles. Samples of TNT particles seeded on a sapphire substrate were scanned and illuminated within the near field using 400 and 266.7 nm pulses. The transmitted signal was monitored with a photo detector and then used to form images. Experiments on individual TNT crystals, where no NSOM images were recorded, were performed in transmission mode using a tip aperture of approximately 1 μm in diameter (figure 18).

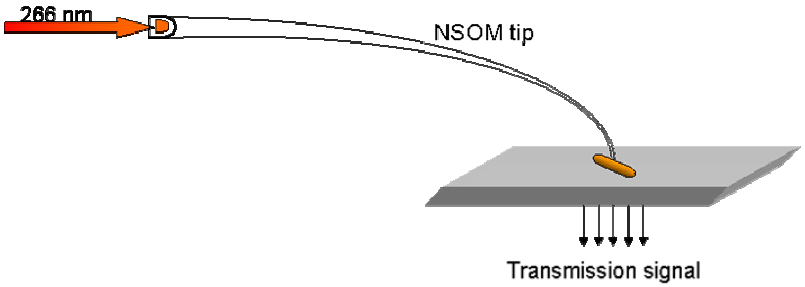

Figure 18. *Near field scanning optical microscopy (NSOM) in transmission mode for individual crystals TNT photoluminescence.*

5. RESULTS AND DISCUSSION

5.1 Photochemistry of TNT in solution.

The clear aqueous and alcoholic TNT solutions turned to yellowish-reddish colored solutions upon exposure to the incident 266.7 nm photons as illustrated in figure 19. TNT in toluene solutions remained colorless after photon exposure.

5.1.1 Photochemistry of aqueous TNT solutions

Aqueous TNT solutions were found to turn yellow upon irradiation with 266.7 nm photons for 5 minutes. The UV-visible absorption spectrum of irradiated TNT in water is markedly different to the spectrum of non-irradiated samples. Figure 20 illustrates the UV spectrum of TNT in aqueous solution that was measured before and after exposure to 266.7 nm photons. A weak shoulder can be identified at about 300 nm in the UV-visible spectrum of non-irradiated samples; while a high wavelength shoulder below 400 nm and a long tail that extends to 600 nm are the most prominent features in the optical absorption spectrum of irradiated aqueous TNT solutions.

Surface reflection Fourier transform infrared absorption (SRFTIR) measurements on deposits of the aqueous TNT solutions were performed with the purpose of establishing their photochemically induced products. Results of the SRFTIR measurements between 600 and 4000 cm^{-1} of 5 μL deposits of non-irradiated and irradiated aqueous TNT solutions are displayed on figures 21 and 22, respectively. Strong absorption bands due to C-C and NO stretching modes are observed between 1000 and 2000 cm^{-1}.

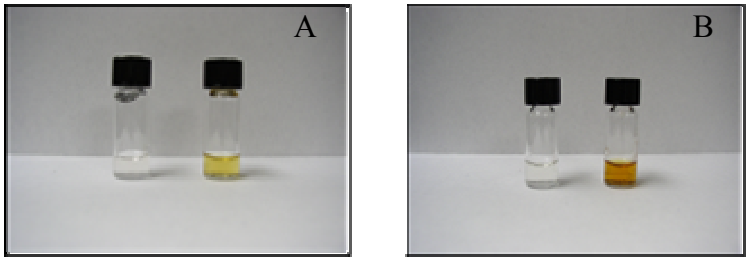

Figure 19. *Comparison of colors of aqueous (a) and alcoholic (b) TNT solutions; before (left flask) and after (right flask) 266.7 nm irradiation.*

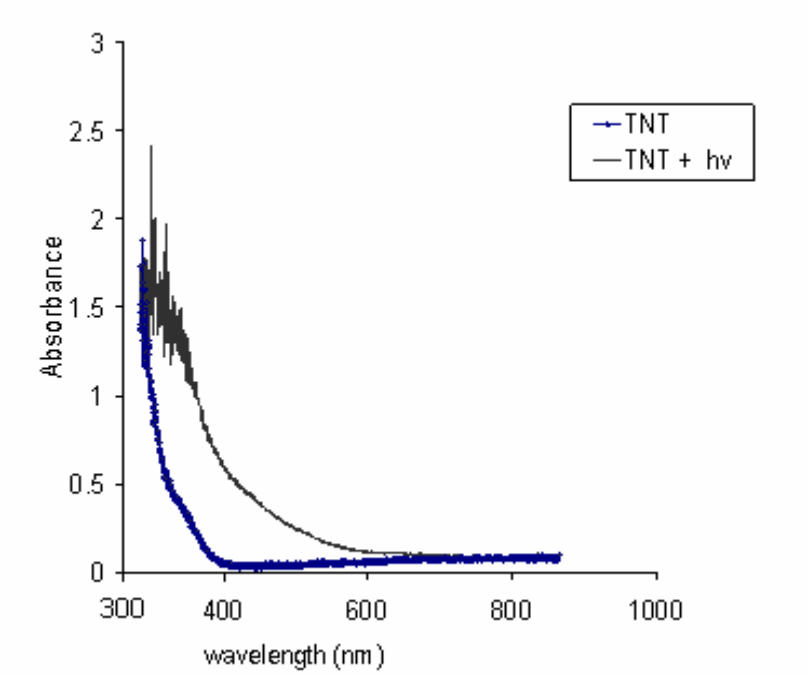

Figure 20. *Comparison of the UV-visible absorption spectra from aqueous TNT solutions before (TNT) and after (TNT+hv) irradiation with 266.7 nm photons.*

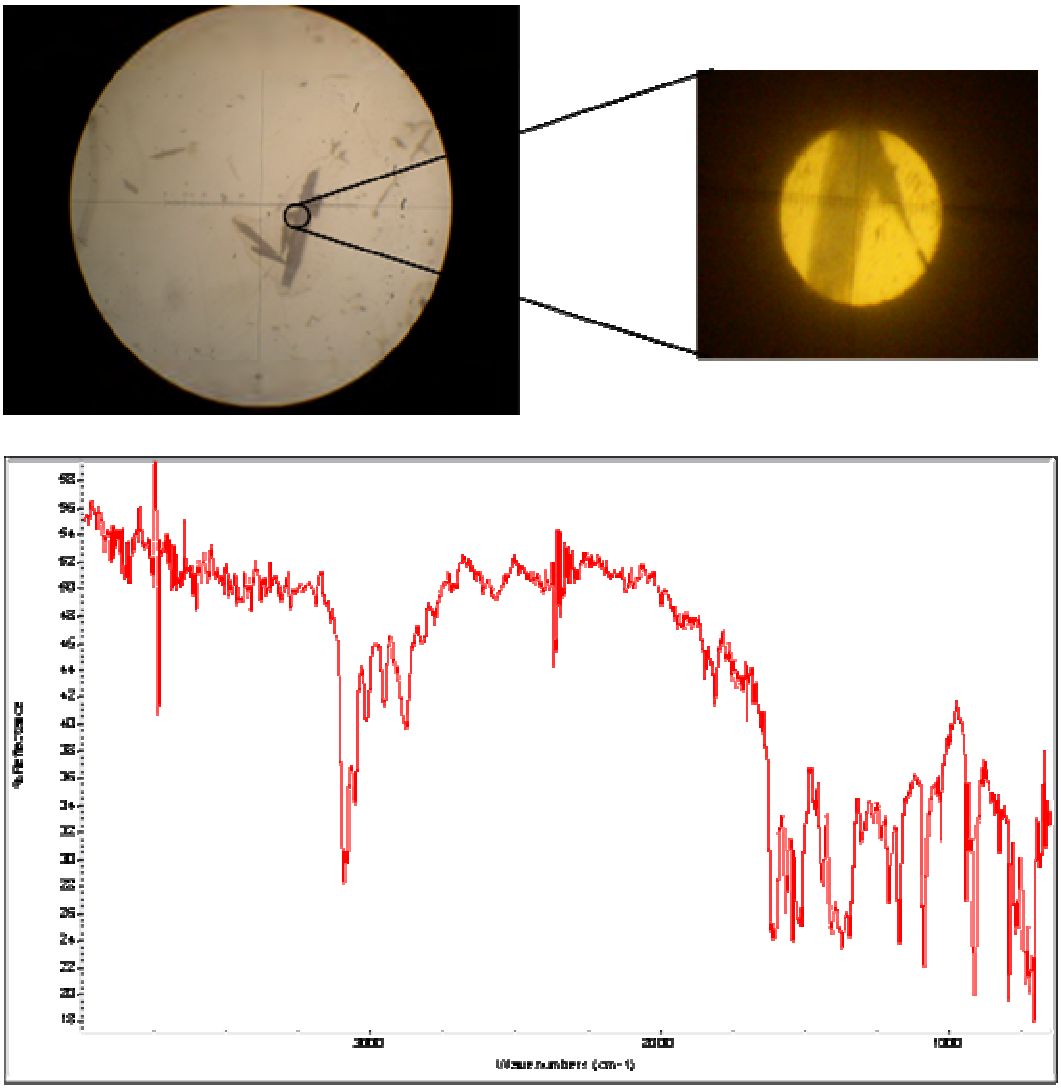

Figure 21. *20X optical image of crystals formed from dried deposits of non-irradiated aqueous TNT solutions (up). SRFTIR spectrum of the crystal showed in the zoomed area (down).*

The vibrational spectrum of deposits of non-irradiated aqueous solutions is consistent with the spectrum of TNT crystals reported in the literature [Clarkson et al. 2003]. Strong bands due to C-H bond stretching modes in the methyl and aromatic parts of the molecule are observed between 2700 and 3100 cm^{-1}.

Crystals in a yellow material are observed in optical microscopy measurements of deposits of irradiated aqueous TNT solutions (figure 22). SRFTIR spectra were measured specifically on those crystals as well as on the yellowish dispersed material. The spectrum of the crystals resemble the typical SRFTIR spectrum for deposits of diluted aqueous TNT samples, this is consistent with a decrease in TNT concentration. In addition, broad absorption bands between 3600 and 2700 cm^{-1} and around 1050 cm^{-1} are noticeable in the post-irradiation resultant crystals. The appearance of these bands is consistent with the formation of alcohols and amines, though the broadness of the bands is more consistent with the formation of alcohols.

Vibrational analysis of the yellow region of the deposits reveals a spectrum with broad absorption bands between 3800 and 2700 cm^{-1}, and also bands centered at 1640 cm^{-1} (C=C stretch), 1450 cm^{-1} (CH_2 deformation) and 1091 cm^{-1} (C-N or O-H deformations) and 776 cm^{-1} (fingerprint of N-H bending mode) [Sadtler 1978]. These bands are not observed in the spectrum of non-irradiated TNT. The appearance of broad absorption bands may result from extensive hydrogen bonding or the formation of multiple photoproducts.

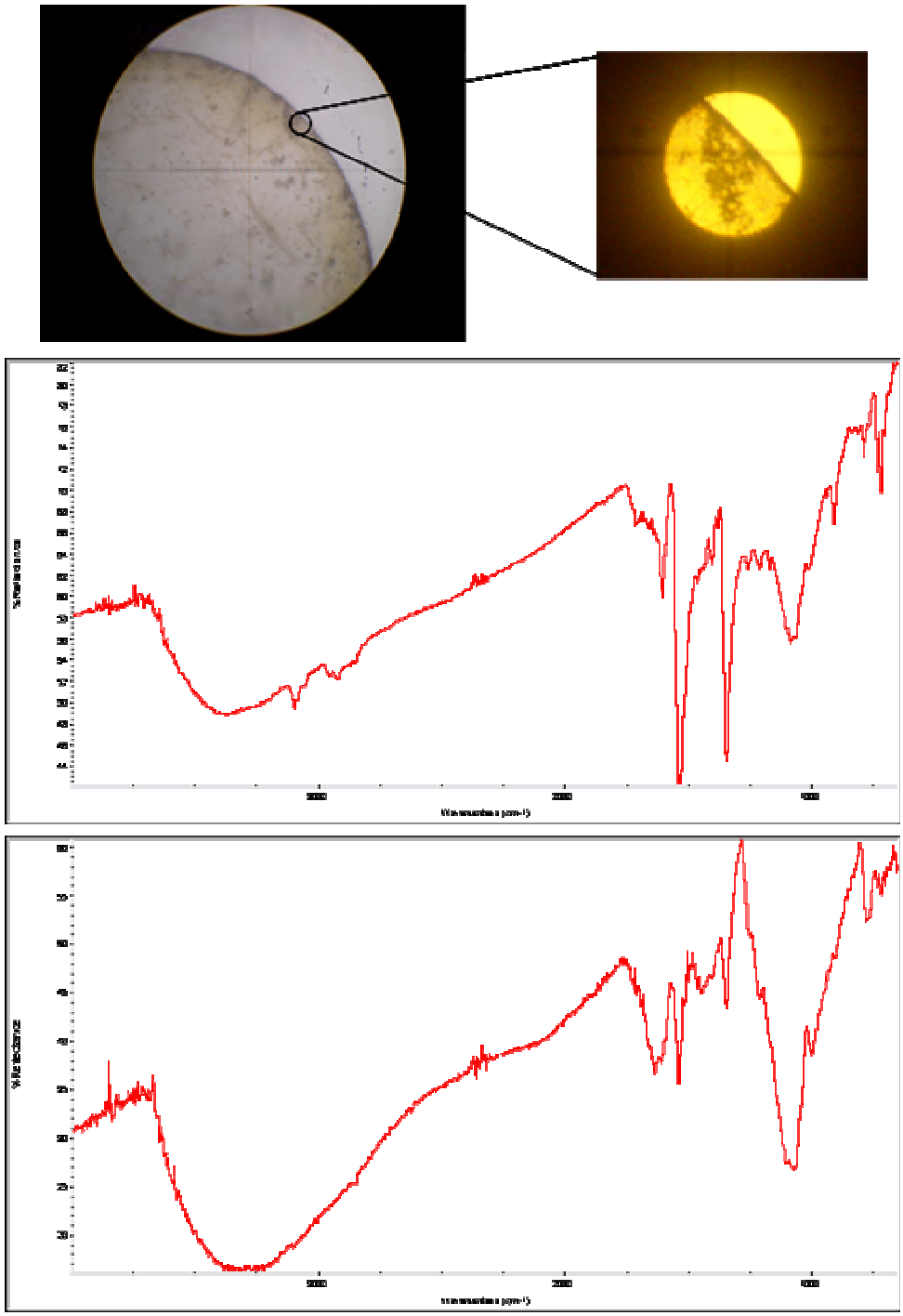

Figure 22. *SRFTIR measurements of dry deposits of irradiated aqueous TNT solutions. Upper and lower curves correspond to crystals and yellow materials respectively found in optical measurements of the dry deposits (see inset).*

5.1.2 Photochemistry of alcoholic TNT solutions

With the purpose of establishing the role of the solvent in the photochemistry of TNT, we have extended our measurements to alcoholic and toluene TNT solutions. The UV-visible absorption spectra of TNT in methanol solutions before and after irradiation are displayed in figure 23. As in the aqueous solutions, the UV-visible absorption spectrum of TNT does not have much structure between 200 and 800 nm save to a long tail that extends to 400 nm. A completely different spectrum is observed in the irradiated samples. There is a well defined peak at about **435** nm and a shoulder at about **510** nm.

SRFTIR measurements were also preformed on dry deposits of this solution with the purpose of identifying the products of the photochemistry of alcoholic TNT solutions. Dry deposits of alcoholic TNT solutions are displayed on figure 24. They resemble a "school of fish" crystal habit for TNT growth [Mc Crone 1993].

The results of vibrational measurements performed on the sample, shown on figure 24, reveal the C-C stretching vibrations of tetra-substituted benzene are around 1602 cm^{-1}. Nitro groups, disturbs the C-H deformation vibrations of ring hydrogens out of the plane of the molecule, therefore in TNT they are around 791 cm^{-1} instead of around 700 cm^{-1}. The absorption bands between 3100 cm^{-1} and 3000 cm^{-1} result from stretching oscillations between H atoms and non-saturated C atoms. Signals at 2950 cm^{-1} and 2880 cm^{-1} are due to C-H stretching modes in the methyl group of TNT. The most intense lines around 1530 cm^{-1} and 1340 cm^{-1} are due to C-NO_2 asymmetric and symmetric stretching vibrations respectively [Sadtler 1978].

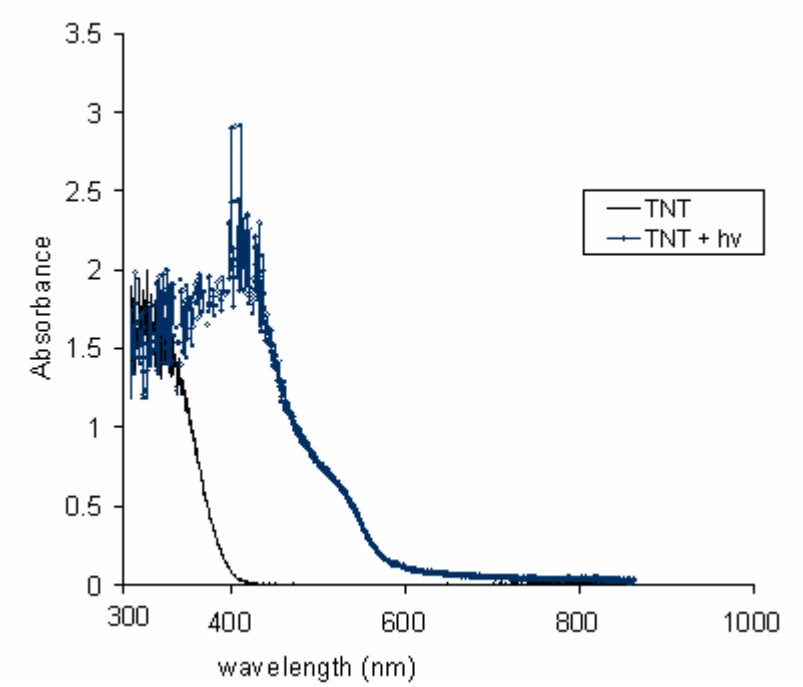

Figure 23. *UV-visible absorption spectra of alcoholic TNT solutions before (TNT) and after (TNT+hv) irradiation with 266.7 nm photons.*

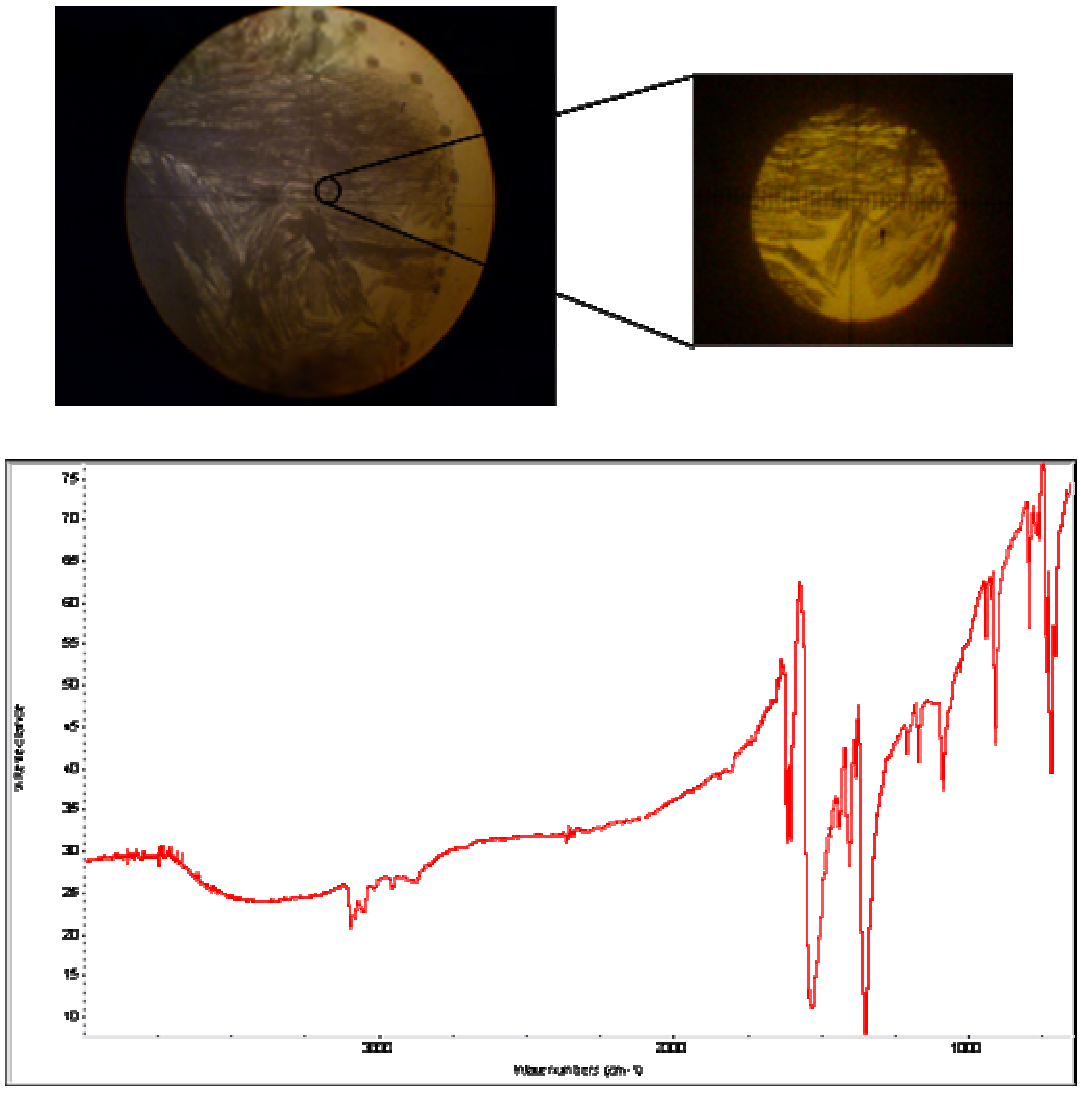

Figure 24. *White light imaging (up) and SRFTIR spectrum (down) of dry deposits of TNT solution in methanol before irradiation with 266 nm photons.*

Figure 25 shows the appearance of 266.7 nm photodecomposition products of alcoholic solution of TNT. Intense orange to reddish crystals were observed in white light imaging measurements. SRFTIR spectrum corresponding to the amplified zone reveals a broad band centered at about 3450 cm^{-1}, which coincides with the N-H stretching mode found in amines. Aromatic and aliphatic C-H stretch remains in the sample but with a relative increase of 2931 cm^{-1} peak with respect to other absorption bands in the regions, suggesting the relative increase of aliphatic C-H vibrations when compared to non irradiated TNT.

It was observed that the difference in intensity between the aromatic and aliphatic (near to 2900 cm^{-1}) C-H signal decreases as time of irradiation increases (analysis not shown). Depletion of the peak corresponding to aromatic C-H stretching at 3104 cm^{-1} was also observed. The presence of a new absorption band located at 1720 cm^{-1} is evident in the spectrum; this strong signal may be characteristic of the C=O stretching mode and may result from the formation of formaldehyde (a side product of methanol decomposition). The intensity of this band increases with irradiation time (analysis not shown). There is the growth of a small band at 1131 cm^{-1} which could result from C-O stretch or a shifted C-N stretch.

All these suggest the formation of a compound mixture, in which some products have a very similar chemical structure to TNT derivatives where it loses nitro groups and/or the molecule itself is reordered aided by the strong stimulation impinged by the femtosecond laser pulses. Besides, there are some photoproducts that have included some of the groups mentioned above such as carboxylic nitro aromatics derivative, amino nitroaromatics and/or nitroaromatic esters.

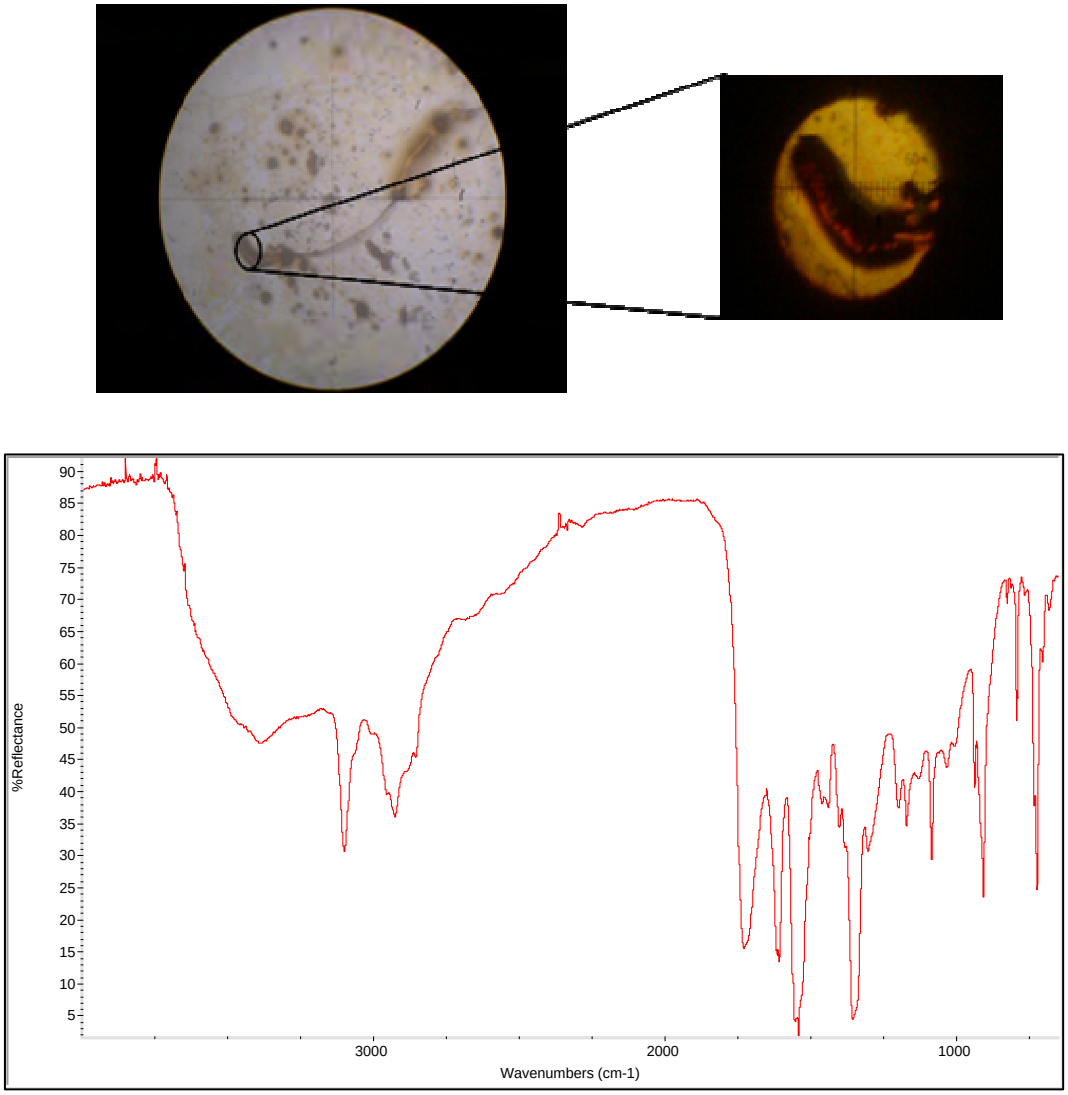

Figure. 25. *White light imaging and SRFTIR measurements of dry deposits of irradiated alcoholic TNT solutions.*

5.1.3 Photochemistry of TNT in toluene

The UV-visible absorption of TNT in toluene solutions before and after exposure to 266.7 nm photons is shown in figure 26. Within the resolution of the spectrograph employed for the measurements, we cannot observe any difference in the UV-visible absorption bands of TNT in toluene between the non irradiated and irradiated samples.

White light imaging and SRFTIR spectra of dry deposits of TNT in toluene solutions before and after irradiation are shown in figures 27 and 28, respectively. As was established by UV-vis analysis, no obvious changes are detected in the structure of the vibrational spectrum of TNT exposed to UV radiation when is compared to non-irradiated TNT.

The results obtained so far, for the photochemistry of TNT in solution, makes obvious that the photodegradation of TNT is strongly influenced by its surrounding medium, as mentioned by several authors. Some have pointed to the direct participation of the solvent and others have proposed that TNT media participate indirectly as a sensitizer for photochemical transformation [Brannon and Pennington 2002].

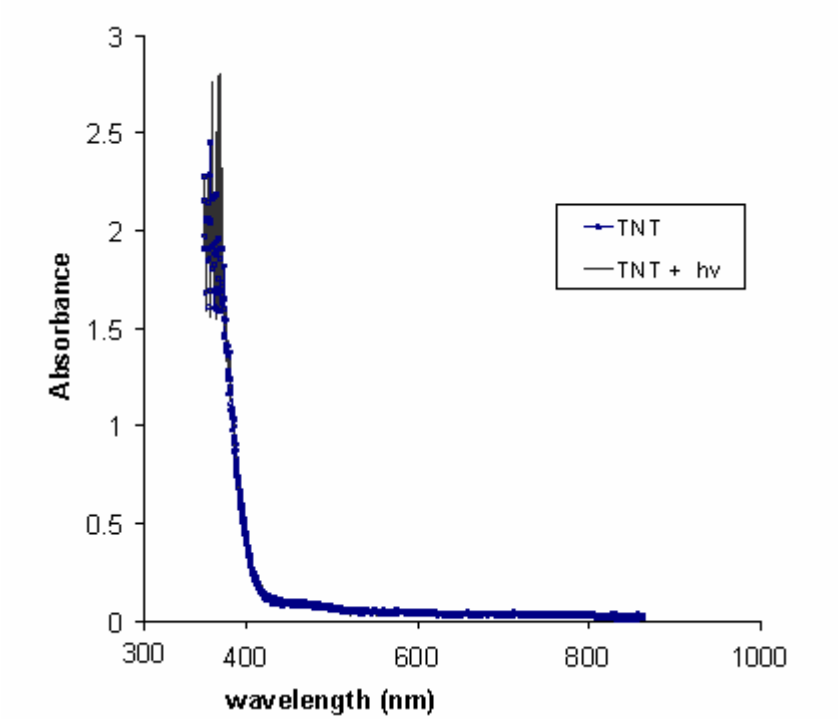

Figure 26. *UV absorption spectra of TNT dissolved in toluene before and after irradiation with 266.7 nm photons.*

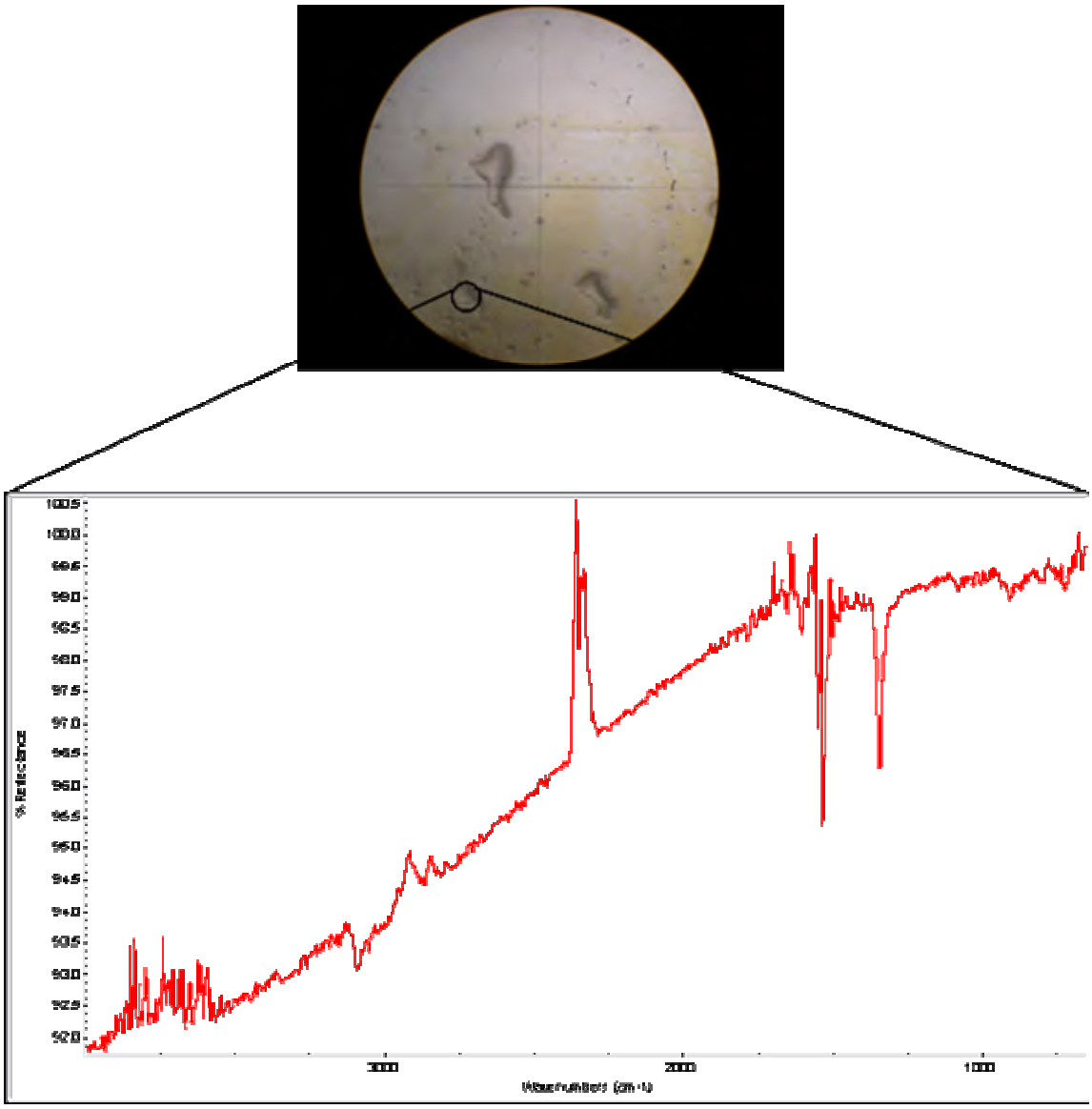

Figure 27. *White light imaging and SRFTIR measurements taken from dry deposits of TNT solutions in toluene before irradiation with 266.7 nm photons.*

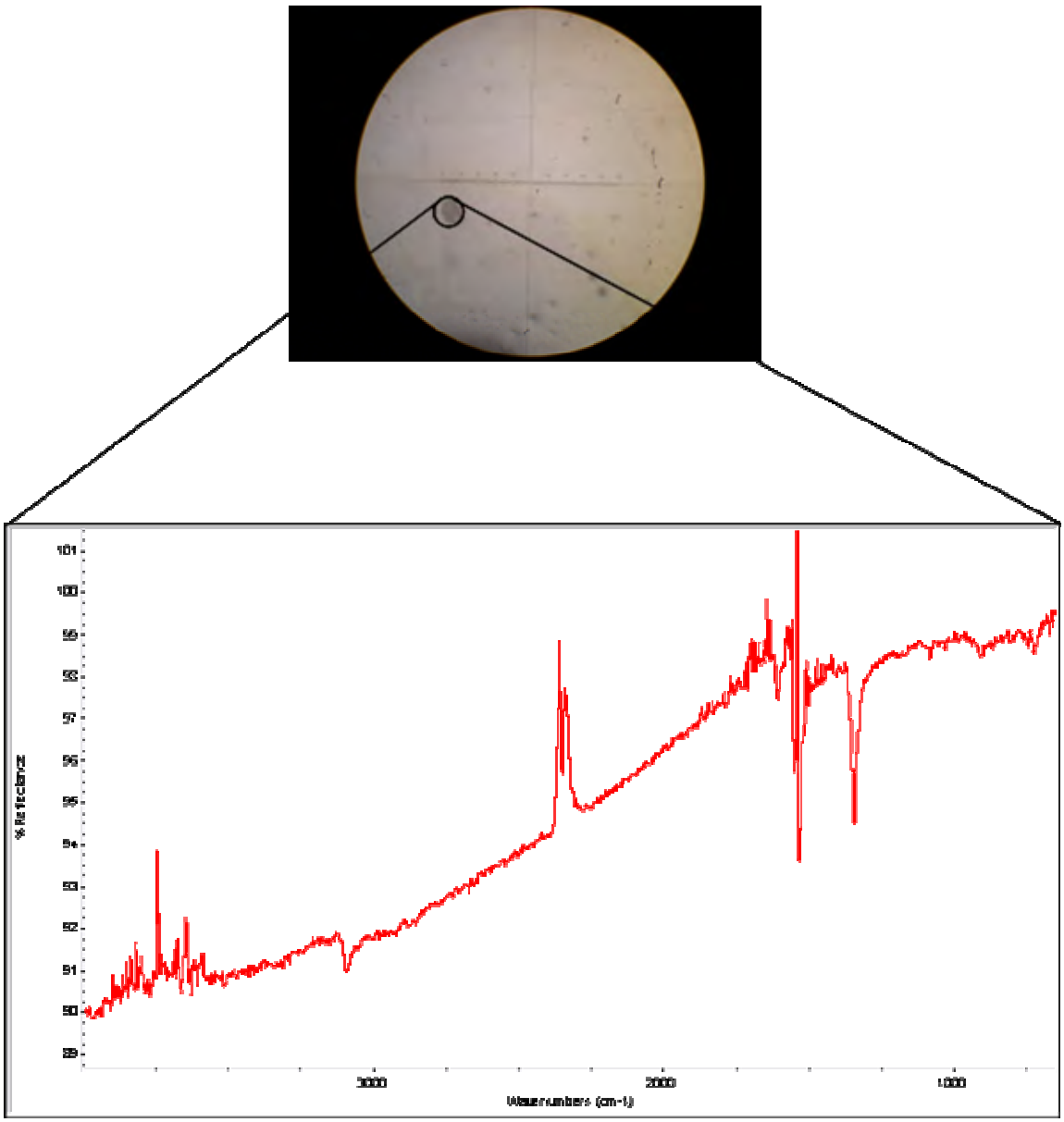

Figure 28. *White light imaging and SRFTIR measurements taken from dry deposits of TNT solution in toluene after irradiation with 266.7 nm photons.*

In this section, significant evidence has been presented for the photodecomposition of aqueous and alcoholic TNT solutions; meanwhile in toluene, the photodegradation of TNT resulted negligible. Several reasons can be attributed to this effect; in this case, the ability for the solvent to donate hydrogen atoms surges as a major fact in this issue due to the very characteristic process of hydrogen abstraction in nitroaromatics photochemistry. Nitroaromatics have been probed to be excellent photo-oxidizers of hydrogen-donor molecules. For instance, solutions of nitrobenzene in methanol are photoreduced via formation of hydroxylamines, consistent with hydrogen abstraction from the solvent; phenylhydroxilamine was identified as the major final product, as well as *p*-nitrophenol, which was formed via rearrangement of the phenylhydroxilamine [Feuer 1970]. This mechanism sufficiently explains the appearance of amines, phenols and aldehydes groups in the photodecomposition products of irradiated aqueous and alcoholic solutions of TNT by oxidizing the hydrogen-donor solvent. In irradiated TNT solutions dissolved in toluene none of the mentioned groups appeared, which can be explained by considering the nature of toluene as a poor hydrogen donor compared to methanol and water.

The solvent nature plays a major role in the formation of the photolysis products of TNT. It was evidenced by the vibrational spectroscopy analysis performed on the dry deposits of irradiated solutions in the solvents used. The appearance of the characteristic vibrational bands of acids/aldehydes, alcohols/phenols and amines, among others TNT photoproducts, agrees with the findings of Burlinson [Burlinson et al. 1979]; where TNT photolysis strongly depended of the solvent pH value. Then, the percentage of the photodecomposition was found proportional to the solvent causticity. In our results both, water and methanol, unlike toluene, have the capability to act as a base in chemical reactions, providing OH^- groups. This group can efficiently facilitate the formation of the Trinitrobenzyl anion by reacting with the photoexcited “Aci-TNT” (see figure 7) and, in this way, generate photoproducts. On the other hand toluene, with low capacity to generate strong basic groups, makes this

path unfavorable and the formation of photoproducts by this route is negligible as confirmed by UV-vis and vibrational spectroscopy.

The presence of parallel mechanisms for TNT photodegradation may not be disregarded. The sensitivity of TNT to bases is well known, color changes in solutions containing nitrobenzenes and appropriate nucleophiles (in this case, OH^-) may indicate the formation of complexes produced by nucleophilic addition to the electron-poor aromatic ring, which then ejects a suitable leaving group such as NO_2 [Larson et al. 2000]. The electron-withdrawing nitro groups deplete the aromatic ring of electron density, imparting to it the properties of an electron pair acceptor. Hence, the nitroaromatics are susceptible to nucleophilic substitution [Lipczynska 1992].

2,6-DNT and Trinitrobenzene have been reported as the TNT major photodecomposition products via alkaline hydrolysis [Emmrich 2001]. Then, this could be a viable mechanism for which colored products would have been formed in aqueous and alcoholic solutions. In toluene TNT solutions, this mechanism is less likely due to the absence of the oxygen atoms needed for the nucleophilic addition of the OH^- group. These results strongly suggest that the solvent is involved in the photochemistry of TNT, either by direct participation in the photochemical process or by providing protons that can hydrogenate excited TNT states; and that the photodegradation of TNT in a solvent like toluene was negligible and could not be appreciated by the analytical techniques used. This was attributed to both, the absence of oxygen in the molecule to facilitate the formation of hydroxyl groups and to its poor hydrogen-donor nature. In both cases the formation of photodecomposition products, by the suggested mechanisms, was largely unfavored.

According to the results obtained so far, the photolysis of pure traces of TNT in air is expected to fragment the molecule to generate NO due to the absence of a hydrogen-donor rich media that surrounds TNT.

5.2 PHOTOCHEMISTRY OF PURE TNT

5.2.1 Synthesis and characterization of TNT nanoparticles

Figure 29 shows the AFM image of a 10 x 10 μm area corresponding to a room temperature (A) and high-energy (B) deposition of TNT particles. At room temperature, the formation of non well-defined shape droplets is observed. Droplets are about 1700 ± 600 nm in diameter and 212 ± 100 nm in height. They seem to have a nearly circular shape but a closer view reveals that TNT particles dispersed on the substrate are not spherical; rather, they adopt an ellipsoidal shape as was confirmed by cross section analysis (figure 30). Elongated-shaped particles are formed in a few regions, a formation attributed to the alignment of several particles. Part B of figure 29 shows the AFM image of a typical high energy deposition. Distinguishable particles are dispersed on the deposition area, which is also dominated by completely amorphous TNT formations. TNT particles are 1300 ± 500 nm in length and 200 ± 99 nm in height.

Figure 30 shows a cross section analysis from a detailed frame of a 10 x 10μm area where rings as the one assigned in the figure has a diameter of ~1500 nm. Particles, as small as 433 nm in diameter, are present in the surroundings of the rings.

SEM images of TNT particles deposited on glass substrates are displayed on figure 31. Images A and C correspond to deposits that were prepared from a room temperature aerosol, while B and D were obtained by warming the aerosol on its flight to the substrate surface with a hot jet of nitrogen gas. Analysis of the SEM images to compare the size distribution of TNT particles deposited at different temperatures confirms that the particles deposited with an aerosol warmed on its flight to the target are smaller than those prepared with a room temperature aerosol.

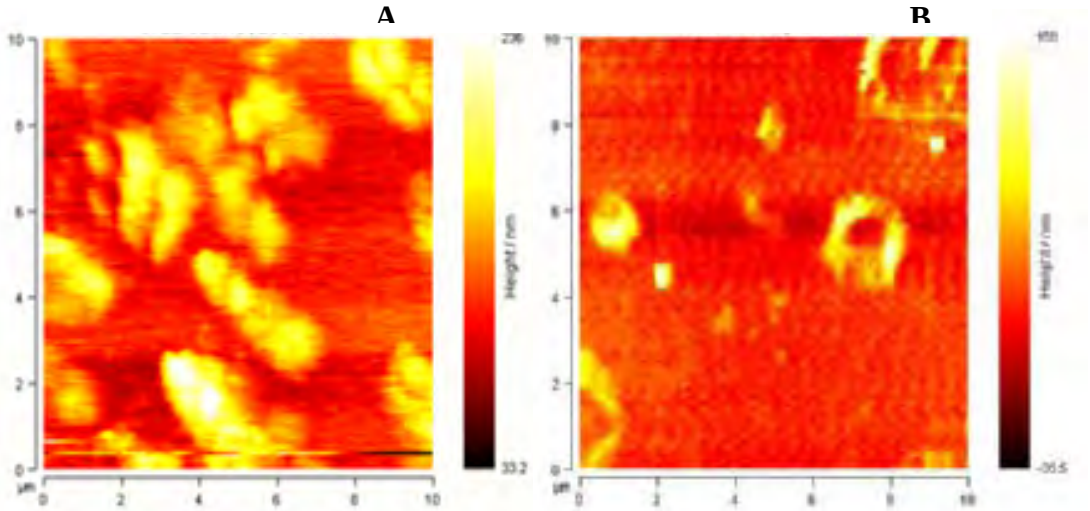

Figure 29. *AFM image of a 10 x 10 μm area from TNT particles deposited at 300 K (A) and 328 K (B). Ring-like formations as well as elongated and nearly rounded particles of less than 1 μm in diameter are present on the surface.*

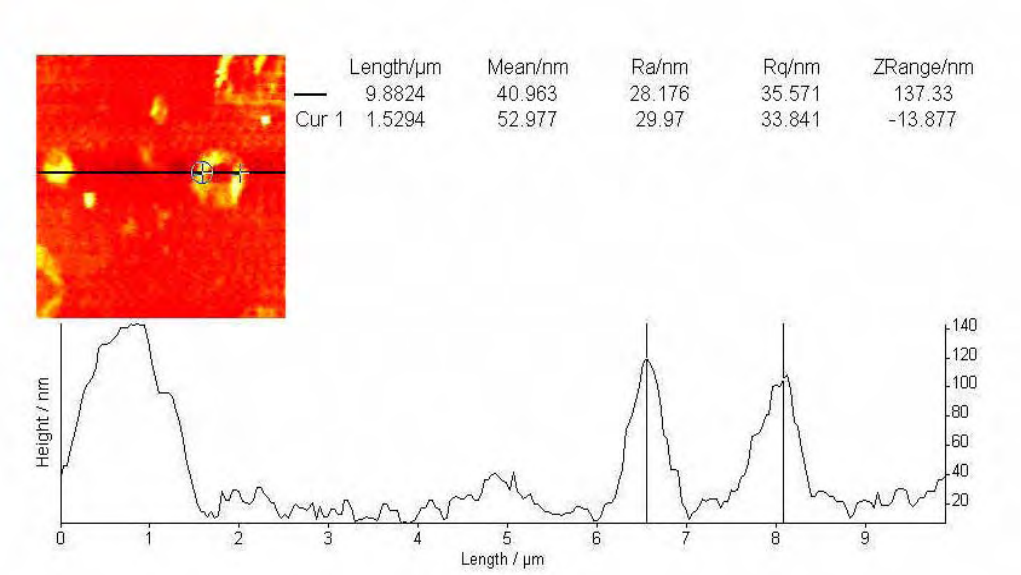

Figure 30. *Cross section analysis of a TNT ring formed using heated nitrogen as drying gas.*

The high energy jet aerosol of methanol-TNT produced smaller TNT formations than room temperature aerosol. The amount of energy transmitted to TNT aerosol by the 328K gaseous nitrogen current allows a fast evaporation of the solvent in the time of flight to the substrate, before hitting it. When the 293K gaseous nitrogen current was used, the energy transmitted to TNT aerosol is not sufficient to induce an effective evaporation of the solvent in the aerosol; most of the solvent was evaporated after the emulsion hit the glass surface. This fact favors the formation of bigger agglomerations of TNT when the colder drying current was used.

Energy dispersed X-ray analysis (figure 32) reveals the presence of small peaks due to carbon, nitrogen and oxygen in the sample, corresponding to the elemental composition of the seeded TNT nanoparticles. The strong Si and Au signals in the EDS spectrum are due to the elemental composition of the substrate.

Increasing the number of aerosol shots resulted in the formation of larger TNT particles and particle agglomerates. These particle agglomerates were analyzed with surface reflection Fourier transform infrared spectroscopy (SRFTIR). Clearly distinguishable spectrum of TNT can be observed in the FTIR measurements (figure 33). Bands due to the symmetric and asymmetric NO_2 stretching modes of vibration are present in deposited particles. Similar spectra are observed in the rings that surround some of the deposits, confirming the presence of the material in the deposits.

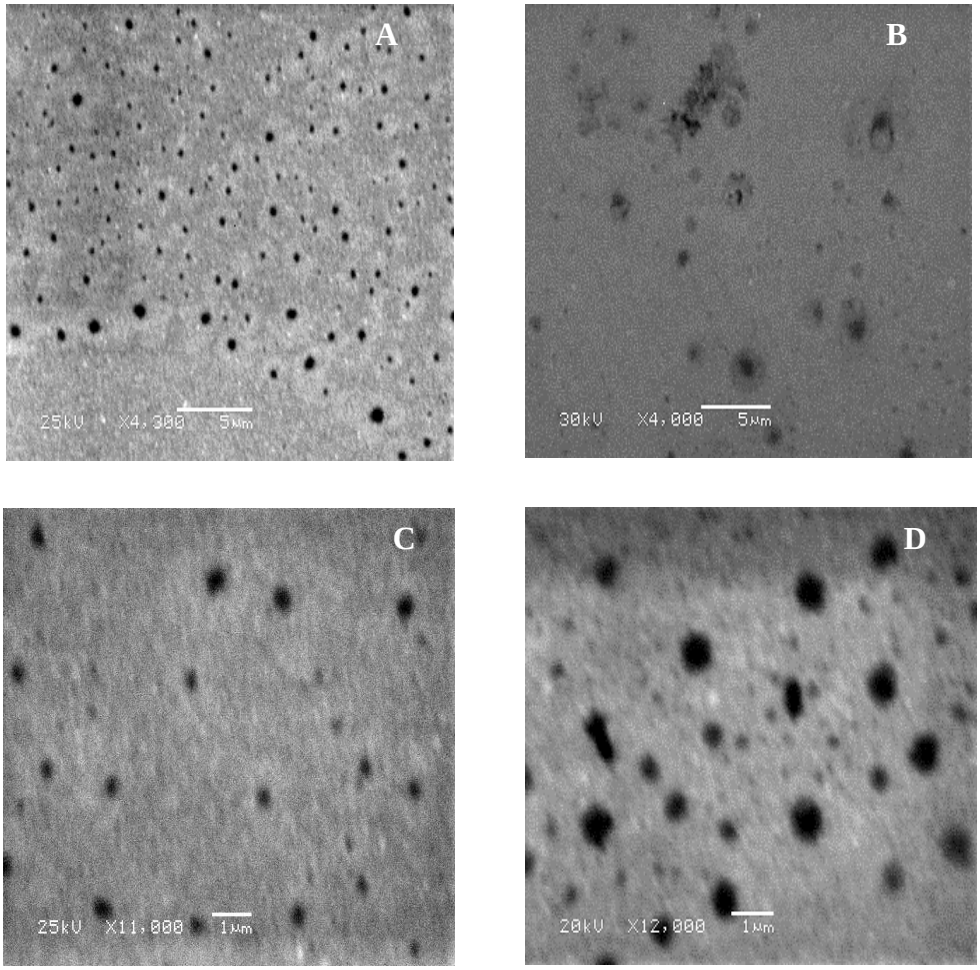

Figure 31. *SEM images of TNT particles prepared from a warmed (A and C) and room temperature (B and D) aerosol jet. The upper and lower images in each case correspond to 5µm and 1µm scales, respectively.*

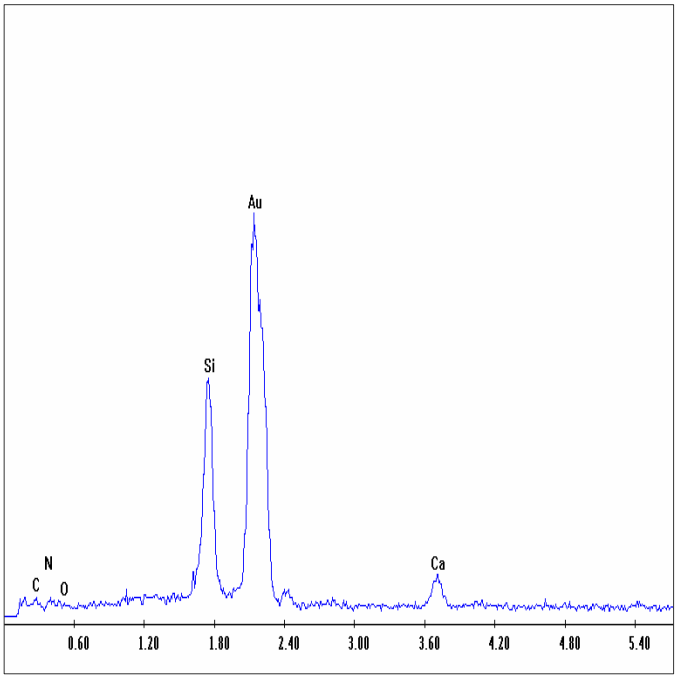

Figure 32. *The energy dispersed X ray spectra of TNT particles deposited with an aerosol jet.*

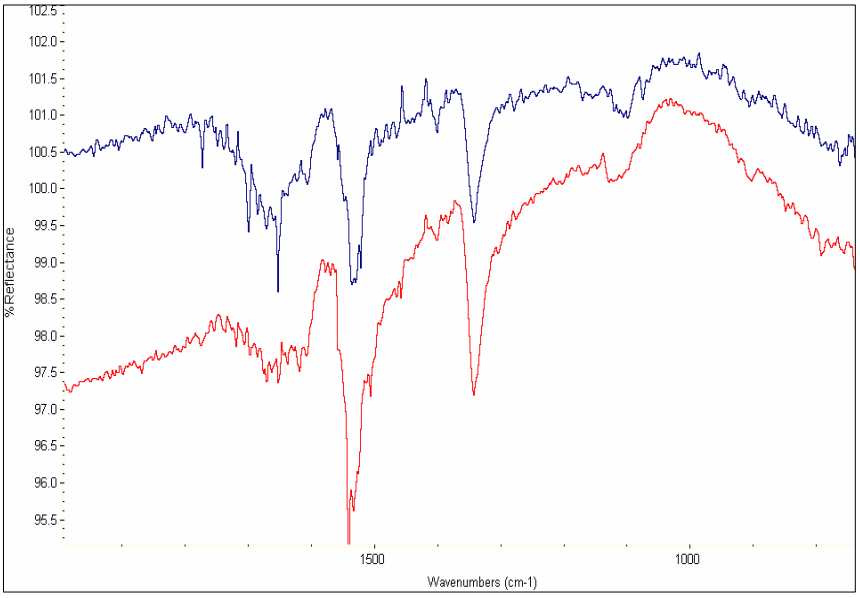

Figure 33 *Surface reflection FTIR spectra of TNT particles deposited with an aerosol jet. The top and bottom surface reflection FTIR traces are obtained in deposits of room temperature and warmed aerosol jets respectively.*

5.2.2 NSOM photochemistry of TNT particles

Near-field scanning optical microscopy (NSOM) images of TNT particles deposited with a warmed aerosol jet were performed, with a transmission mode configuration, using ultrafast laser pulses of 400 nm. The scattered radiation was collected by a microscope and fed into a spectrograph (see figure 17). The spatial distribution of the 400 nm radiation reaching the photomultiplier tube used as the detector was monitored and the signal output fed into the NSOM system for analysis. A tapered fiber optic tip with an aperture diameter of 250 nm was employed for the measurements.

A representative NSOM image of the TNT particles is summarized on figure 34. The 15 x 15 μm image is the result of the interaction between the illuminating radiation and the TNT particles. The presence of TNT particles on the surface scanned is manifested by the brighter zones of the images. This result indicates that a higher transmission of the illuminating photons is obtained while scanning TNT particles at 400 nm. Three different regions were marked on the NSOM image, where transmission spectra were registered between 399 and 402 nm (figure 35). The transmission spectra consist of one strong band centered at about 400 nm, corresponding basically to the laser emission. A zoomed area of the transmitted beam spectra is showed in the inset of the figure 35. It reveals that the peak of the emission band has a defined structure, especially at 401 nm. The intensity of the 401 nm band exhibits the strongest increase while the presence of TNT increases. This supports the color contrast obtained in the NSOM image which assigns brighter colors to the TNT particles.

The results of the NSOM analysis performed on TNT particles with the use of ultrafast pulses at 266 nm are shown in figures 36 and 37. Figure 36 presents both, the topography (AFM) and the NSOM image of TNT deposited onto a sapphire substrate.

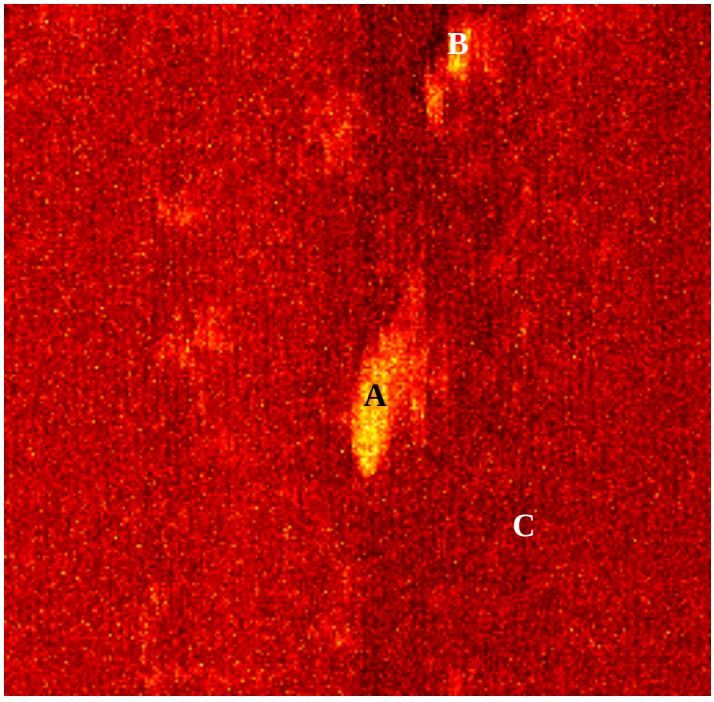

Figure 34. *Transmission 15 x 15 micrometer NSOM scan of TNT particles. TNT particles appear as bright spots on the image.*

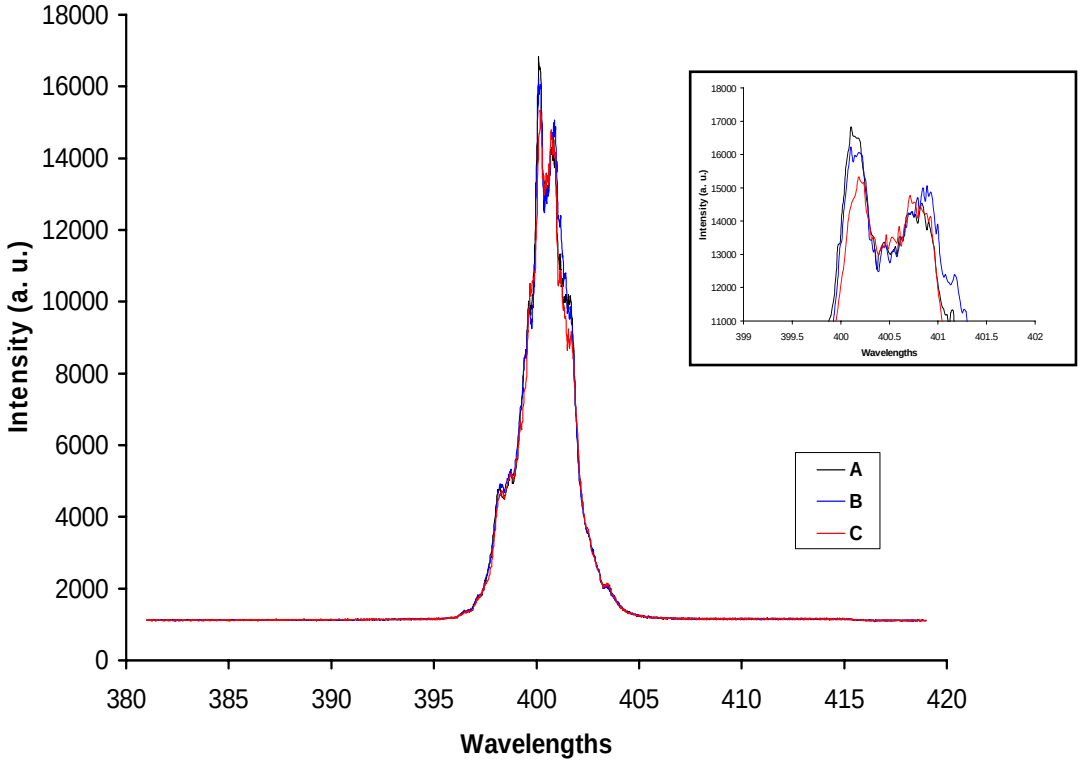

Figure 35. *Transmission NSOM signal of TNT particles. The transmission spectra A, B and C correspond to the indicated points in figure 34. A clear depletion is observed in the 400.1 nm laser peak from A to C.*

The NSOM image of TNT presents a dark contrast for the presence of this compound on the scanned area. This indicates a strong absorption cross section underwent by TNT molecules while irradiated with ultraviolet radiation. In this case, 266 nm photons where found to be useful to unveil the presence of TNT, one of the most photochemically active nitroaromatics.

The difference in color contrast that was obtained from the NSOM analysis of TNT particles at 400 and 266 nm can be explained if it is considered the super-cooled liquid properties that nano and micro sized TNT particles posses. Thus, as TNT does not absorb energy at that wavelength, an irradiated droplet acts as a nano or micro collecting lens, whichever would be the case, intensifying the field that is transmitted through it.

Figure 38 spectroscopically confirms what was optically displayed by the NSOM image. The UV transmission spectra reveal the strong absorption of UV radiation corresponding to the TNT particle, and a complete UV transmission from the sapphire substrate.

For the experiments on individual TNT crystals, the UV-fs laser/NSOM system was used to register the UV transmission spectra of TNT individual crystals. The incident radiation wavelength was 266.7 nm. Figure 38 displays the transmission spectra that were obtained from far-field (bottom) and near-field (top) illumination, using a NSOM tip with a nominal aperture diameter of 500 nm.

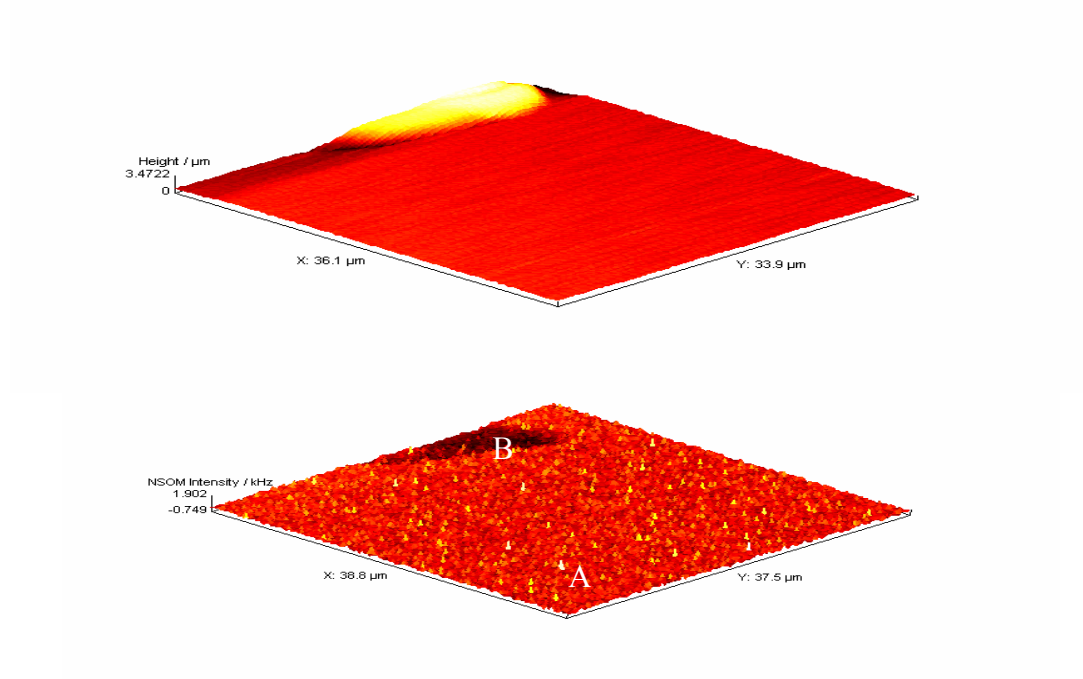

Figure 36. *Topography (up) and NSOM transmission (down) images from a TNT agglomeration seeded onto a sapphire substrate. TNT formations appear as dark contrast in the image. A and B are points were transmission spectra were registered.*

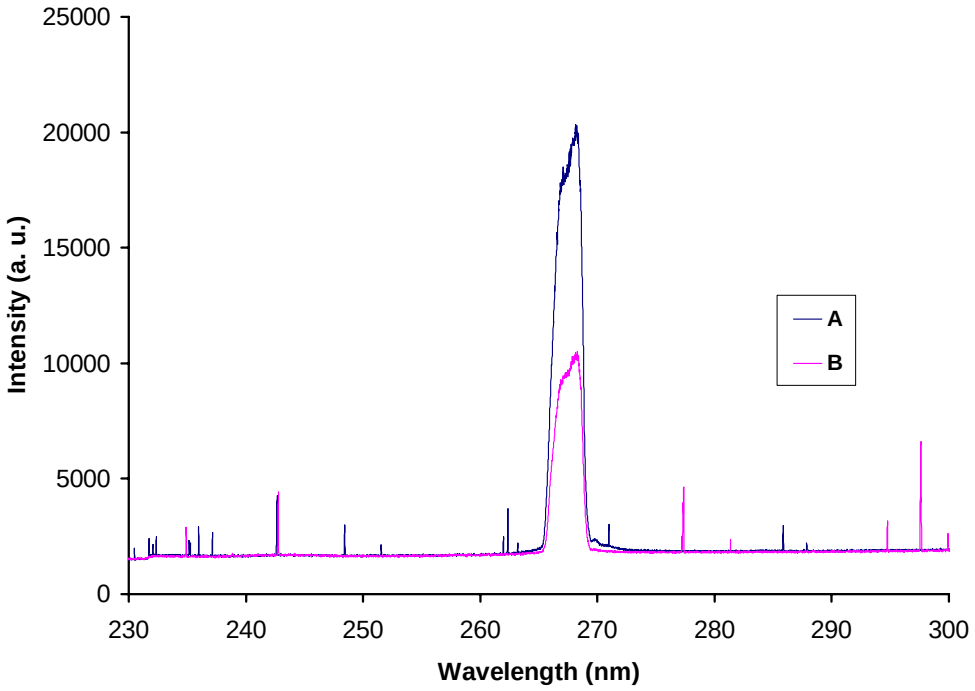

Figure 37. *Transmission spectra of the indicated points in figure 36. Spectrum A corresponds to the background and spectrum B to TNT particles.*

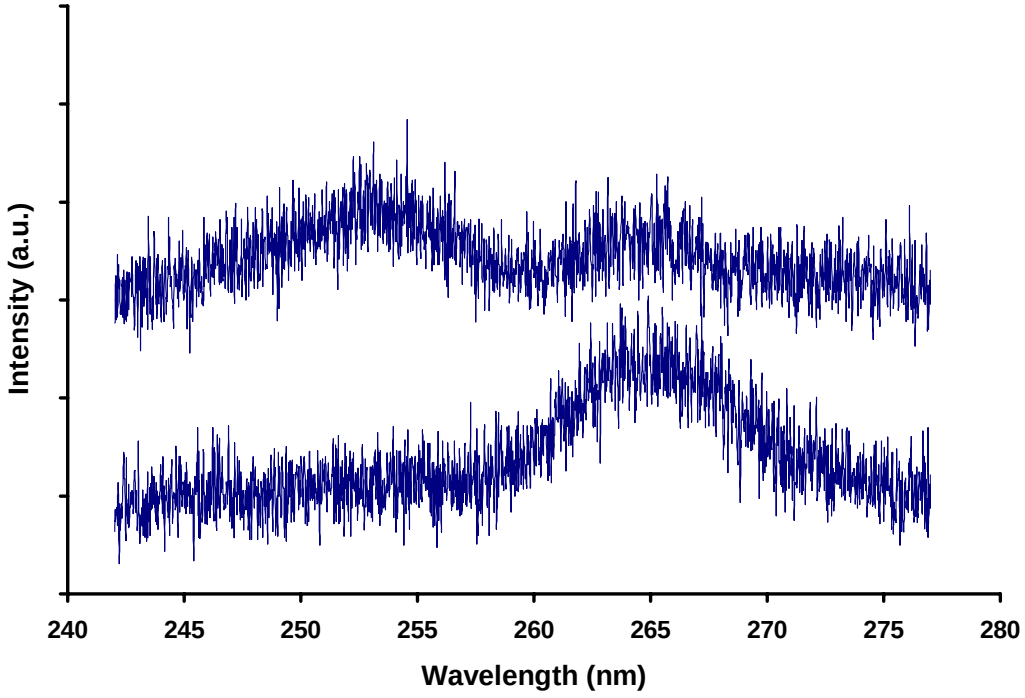

Figure 38. *Fluorescence NSOM spectrum of NO photofragments obtained by irradiation of a individual 2,4,6-Trinitrotoluene crystal from the far field (down) and the near field (up). 266.7 nm fs pulses were used to illuminate the sample.*

The spectrum obtained from measurements with the tip placed out of the crystal near field presents a band due to the incident laser transmission centered at 266.7 nm, for the TNT near-field transmission spectrum, the radiation collected by the spectrograph displays a broad band centered at about 252 nm, in addition to the excitation band at 266.7 nm from the laser, which appears strongly dumped. The band observed at 252 nm can not be accounted for by a light scattering mechanism, since it is centered as a lower wavelength and therefore, higher energy, than the incident radiation. This emission band, at 252 nm, likely results from the fluorescence of NO fragments produced by photo-dissociated TNT [Gomez et al. 2004]. Previous works related to the photochemistry of bulk TNT have reported a similar fluorescence band in this region, with an emission band from about 245 to 250 nm. This band has been observed in one photon and multiphoton absorption experiments around 245 - 250 nm, and is attributed to emission of photofragmented NO. The ground state NO is excited trough $A^2\Sigma \leftarrow X^2\Pi$ (n,0) and hence, produces NO fluorescence trough $A^2\Sigma^+ \rightarrow X^2\Pi$ (2,0) [Shu et al. 2000, Swayambunathan et al. 2000].

The emission band obtained from fluorescence experiments showed a particular behavior of resonance frequency as well as intensity shifting with time. The room-temperature spectral jumps occurs on a long time scale, since appears in spectra obtained with 5 minutes acquisition time and could be up to 5 and 10 nm. This phenomenon is not well understood yet, but it has been reported as being commonly present and characteristic of single-molecule fluorescence experiments. One proposed mechanism for the intensity jumps is the molecular reorientation on the surface that induces configurational changes in the nearby host, affecting the frequency of the electronic transition via guest-host coupling [Moerner 1996, Xie 1996]. TNT molecules as well as its NO photofragments readily sticks to the exposed surface from a Si microcantilever exposed to vapors of these compounds, as has been demonstrated recently [Muralidharan et al. 2003]. Then, the small gap existing between the NSOM silicon-based tip of less than 50 nm and the generation of copious amounts of NO within the near field of a TNT crystal surface, suggest that a guest-

host coupling is possible between the silicon exposed aperture of the NSOM tip and the adsorbed emitting molecules that can induce the observed spectral shifting.

The dependence of the fluorescence signal on the excitation energy is shown in figure 39. The NSOM fluorescence measurements were carried out on a fixed crystal of TNT using five minutes acquisition time. The average of the emission signal resulted to be a non-linear function of the excitation power. A multiphoton process originates when a molecule is excited to a higher electronic state by absorbing two or more photons in the same quantum event. The fluorescence intensity I_{ft} depends on excitation power density ρ_{exc} according to:

$$I_{ft} = \gamma(\varphi_{ft} / i)\, n\mathrm{d}\sigma_i \rho^i \qquad \text{(Equation 2)}$$

In equation 2, γ is a fluorescence collection efficiency factor, (φ_{ft} / i) the one-photon excited fluorescence quantum yield corrected for the multiphoton absorption, n the number density of the absorber, σ_i the absorption cross section for i photons and d the sample path length, and i the number of photons absorbed. From this equation, it can be stated that the logarithm of I_{ft} depends linearly with the logarithm of ρ_{exc} with slope i.

To gain a further understanding of the excitation process, the fluorescence dependence on the excitation power was established. Figure 40 presents the corresponding linear regression fit for the ln-ln plot, which is given by: $\boldsymbol{y = 1.86x - 3.11}$ and its square correlation coefficient: $\boldsymbol{r^2 = 0.9233}$. The observed power dependence, $1 < i < 2$, can be considered consistent with a two photon absorption process. The process of TNT fragmentation and excitation of NO fragments is illustrated in the diagram shown in figure 41. These results can explain the appearance of the fluorescence band at shorter wavelengths than the wavelength used for excitation.

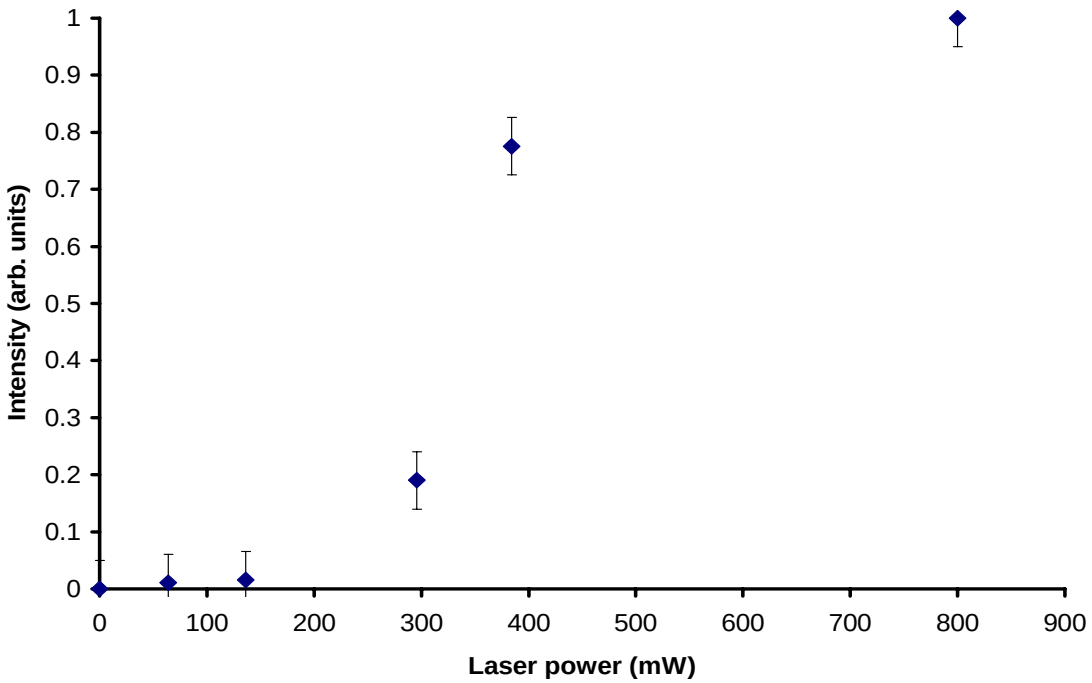

Figure 39. *NO near-field fluorescence signal dependence on nominal laser power. The LP/LIF signal intensities were obtained in one-color experiments at 266.7 nm on individual crystals of TNT, under open conditions at room temperature. Error bars correspond to the 5 percent instability in fs pulses.*

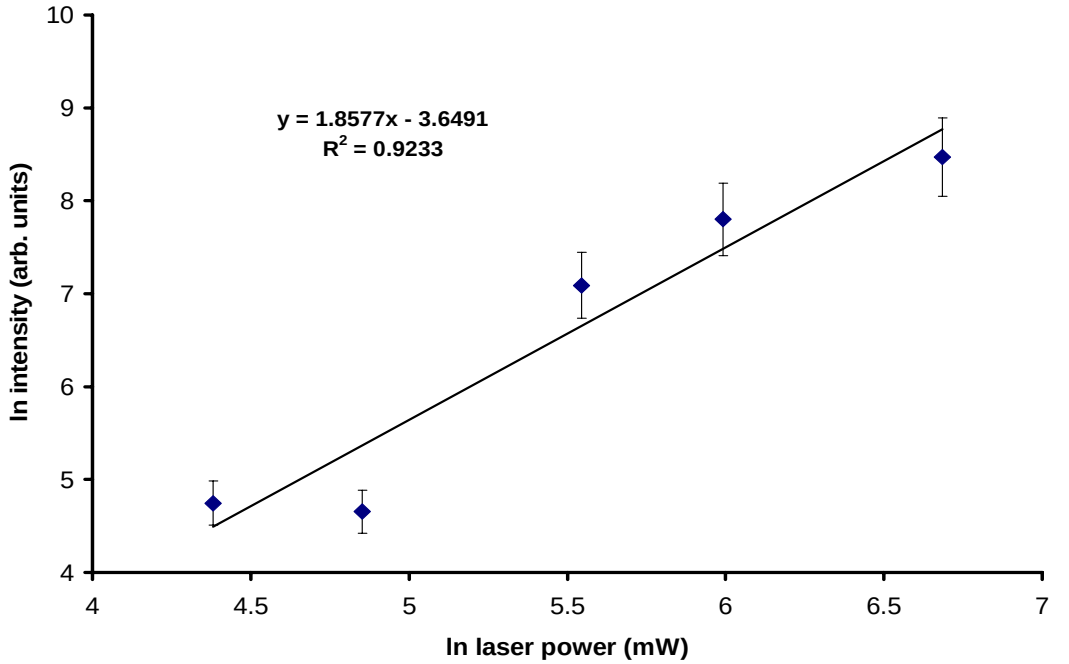

Figure 40. *Double logarithm plot of NSOM fluorescence as a function of laser power for photodissociated NO from TNT individual crystals.*

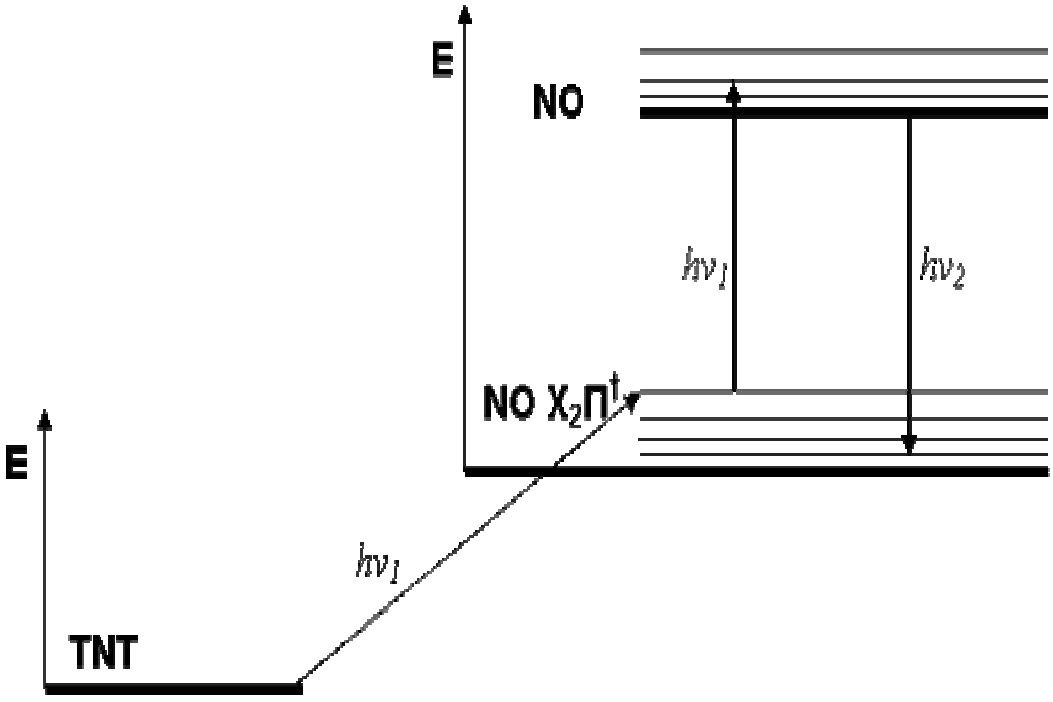

Figure 41. *Diagram to illustrate the multiphoton absorption process involved in the NSOM fluorescence emission from TNT crystals. TNT molecules absorb one photon (hv_1) when irradiated in the near field to produce vibrationally excited NO* ($X_2\Pi^i$). *Then, it absorbs a second photon to reach the electronically excited state* ($A_2\Sigma^*$) *from where fluorescence emission is achieved (hv_2).*

6. CONCLUSIONS

The formation of colored products in the photolysis of aqueous TNT solutions strongly depends on the solvent used, which plays a major role in the formation of the photolysis products of TNT solutions.

Aqueous and methanol TNT solutions readily produce colored compounds upon irradiation with UV photons while toluene TNT solutions do not generate colored products. This is attributed to whether, the absence of oxygen in the molecule to facilitate the formation of hydroxyl groups that consequently can hydrolyze the molecule or to its poor hydrogen-donor nature, compared to the others solvents used, that prevents hydrogen abstraction processes. In both cases the formation of photodecomposition products, by the suggested mechanisms, is largely unfavored.

The use of ultrafast laser systems for TNT detection is encouraged by the results presented here which may have important implications on TNT detection in wet environments.

A Femtosecond pulsed laser-NSOM coupled system can be used to obtain photochemical information from TNT dispersed particles and individual crystals. In this work, the study of the photochemistry of pure TNT using this system, has shown that this compound is able to absorb UV radiation when is reduced to nano-scale sized particles; in our case, particles no smaller than 400 nm. It also appears highly transparent to visible wavelengths, which accords with what is already known from the bulk compound.

TNT can undergo a photofragmentation process followed by NO-fragments fluorescence emission when is irradiated within the near field of individual crystalss. The absorption band shifting suggests single molecule fluorescence detection from NO molecules near to the tapered NSOM fiber end. The near-field fluorescence

collected from NO fragments appears in the range of 245 to 255 nm and requires a two photon absorption process for excitation with a 266.7 nm pulsed laser.

The results presented in this thesis related to the photochemistry of bulk TNT had been reported as similar fluorescence band in this region by different authors, but such studies required controlled environmental conditions and inert atmospheres. These, on the contrary, represent a novel approach of measurements of NO fluorescence from traces of TNT in air environments.

7. FUTURE WORK

Further work is recommended to provide more evidence about the solvent role in the photolysis of TNT. The study of the extent of the solvent participation in the development of colored products, formed due to reduction of TNT in water and methanol, using labeled solvents could be used to better understand this process. Moreover, a comprehensive study seeking the detection of more stable compounds than TNT, formed from TNT photolysis, by the use of the system fs laser / NSOM near field optical spectroscopy could provide an excellent route to trace the presence of landmine explosives in the field.

Experiments that look for the detection of NO, by the photofragmentation/laser induced fluorescence method with the use of NSOM, not only for individual TNT crystals but also for smaller particles, may unveil interesting size dependent optical properties in TNT. Excitation laser wavelength, irradiation distance within the near field, and TNT absorption-desorption on the NSOM tip at controlled temperature conditions are some of the variables to be studied in order to fully characterize the nature of the fluorescence signal detected by the coupled system fs laser/NSOM.

Additional work directed to better the stability of the coupled fs-laser/NSOM system that was developed in this work, will reduce the number of variables to take into account for data analysis. This may also allow the study of non-volatile photoproducts of TNT, in order to make TNT detection in open environments more effective.

8. BIBLIOGRAPHY

Albini A. and Fagnoni M. *Green Chem.* 6, 1, (2004)

Bernasconi C. F. *J. Org. Chem.* 36, 1671, (1971)

Betzing E. and Chichester R.J., *Science* 262, 1422 (1993)

Brannon J. M. and Pennington J. *U.S. Army Engineers Research and Development Center.* Annual report (2002).

Bouhelier A., Beversluis M. R. and Novotny L. *Ultramicroscopy,* 100, 413, (2004)

Burlinson N. E., Sitzman M. A., Kaplan L. A. and Kayser E. *J. Org. Chem.* 44, No. 21, 3695 (1979)

Clarkson J., Smith W.E., Batchelder D., Smith D.A. and Coats A. M. *J Molec. Structure* 648, 203 (2003)

Colling J *Mines and Mine clearance*, Colling King ed, 1999-2000.

Courjon, D. *Near-field microscopy and near-field optics* London: Imperial College Press, (2003).

Dunn R.C. *Chem. Rev*., 99, 2891 (1999)

Emmrich M. *Environ. Sci. & Tech*. 35, 874, (2001)

Feuer H. *The chemistry of the nitro and nitroso groups.* New York, Interscience publishers, (1970) Part I

Fisher M., Cumming C., Fox M., LaGrone M., Jacob S., Reust D., Rockley M., and Towers E. *Nomadics, Inc. white papers* (2000)

Gomez L. M., Santana A., Hernandez S. P., Castro M. Proceedings of SPIE 5415; SPIE proceedings series, Orlando, FL (2004).

George V., Jenkins T. F., Leggart D. C., and Cragin J. H., *Proceedings of SPIE* 3710, 258, SPIE proceedings series, Bellingham, WA (1999).

Hess H. F., Betzig E. Harris. T. D., Pfeiffer L. N. and West K. W. *Science* 264, 1740 (1994)

Jenkins T. F., Legget D. C, Miyares P. H., Walsh M. E, Ranney T. A., Cragin J. H. and George V. *Talanta* 54, 501 (2001)

Jimenez A. M. and Navas M. J. *J. Hazard. Mat.* 106A 1 (2004)

Kenna B.T. and Conrad F.J., *Sandia Report* SAND86-0141, Sandia National Laboratories, 1986.

Larson R. A., Jafvert C. T., Bosca F., Marley K. A. and Miller P. L. *Environ. Sci. & Tech*. 34, 505 (2000)

Lee S-H., Hirokawa J., Kajii Y., and Akimoto H. *Rev. Sci.Instrum.* 68 (7), 2891-2897 (1997)

Lemire G. W., Simeonsson J. B. and Sausa R. C. *Anal Chem.* 65, 529 (1993)

Lewis A., Isaacson M., Harootunian A., and Muray A. *Ultramicroscopy* 13, 227-232 (1984)

Lopez-Martens R. B., Schimdt T. W. and Roberts G.; *J. Chem Phys.* 111 (16), 7183 (1999)

Mc Crone W.C., Andreen J. H., Tsang S–M, *Microscope*, 41, 161, (1993)

Mercado L., Torres P., Gomez L.M., Mina N., Hernandez S. P., Lareau R., Chamberlain T., and Castro M. E. *J. Phys. Chem. B*. 108 (33) 12314, (2004)

Morrison H. and Migdalof B.; *J. Org. Chem.* 30, 3996 (1965)

Muralidharan G., Wig A., Pinnaduwage L.A., Hedden D., Thundat T. and Lareau R. T., *Ultramicroscopy* 97 433 (2003)

Nolan R. and Gravite D.; *Report 2217*, US Army Mobility Research and Development Command, (1977).

O'Keefe J.A. *J. Opt. Soc. Am*. 46, 359 (1956)

Pohl D. W., Denk W. and Lanz M., *Appl. Phys. Lett.* 44, 651 (1984)

Shu J., Bar I., Rosewarks S.; *Appl. Phys. B.* 71, 665 (2000)

Swayambuthan V, Sausa R, and Singh G, *Appl. Spectrosc.* 54, 651-658, (2000)

Sylvia J. M., Janni J. A., Klein J. D. and Spencer K. M., *Anal Chem*. 72, 5834 (2000)

Synge E.H. *Philos. Mag*. 6, 356 (1928)

Synge E.H. *Philos. Mag*. 11, 65 (1931)

Synge E.H. *Philos. Mag*. 13, 297 (1932)

Trautman J. K., Macklin J. J., Brus L.E. and Bezig E. *Nature*, (London) 369, 40 (1994)

Trautman J. K., Macklin J. J., *Chem. Phys*. 205, 221 (1996)

Wayne, R P. *Principles and applications of photochemistry* New York: Oxford, 1988.

Wu D., Singh J. P., Yueh F. and Monts D. L. *Appl. Optics 35,(21) (1996)*

Xie X. S. and Dunn R. C. *Science*, 265, 361 (1994)

Xie X. S., Allen E. V., Holtom G. H., Dunn R. C., L. Mets, *Proceedings of SPIE*: Bellingham, WA. 264 (1994)

Yinon J. *Trends Anal. Chem*. 21, 292 (2002)

Yinon J. *Forensic and environmental detection of explosives*, chapter 6 , John Wiley & Sons, LTD, England, 1999.

APPENDIX

A. List of products from laboratory irradiation of aqueous TNT solutions.

2,2',6,6'-tetranitro-4,4'-azoxytoluene	Burlinson et al. (1973)
4,4',6,6'-tetranitro-2,2'-azoxytoluene	Burlinson et al. (1973)
2',4-dimethyl-3,3',5,5'-tetranitro-ONN-azoxybenzene	Burlinson et al. (1973)
2,4'-dimethyl-3,3',5,5'-tetranitro-ONN-azoxybenzene	Burlinson et al. (1979)
2,4-dinitroisoanthranil	Burlinson et al. (1979)
2,2'-dicarboxy-3,3'5,5'-tetranitroazobenzene	Burlinson et al. (1979); Kaplan, Burlinson, and Sitzmann (1975)
2-carboxy-3,3'5,5'-tetranitro-NNO-azoxybenzene	Burlinson et al. (1979); Kaplan, Burlinson, and Sitzmann (1975)
2-amino-4,6-dinitrobenzoic acid	Burlinson et al. (1979); Spanggord et al. (1980a); Kaplan, Burlinson, and Sitzmann (1975)
4,6-dinitroisoanthranil	Kaplan, Burlinson, and Sitzmann (1975)
Syn-2,4,6-trinitrobenzyl doxime	Kaplan, Burlinson, and Sitzmann (1975)
2,4,6-trinitrobenzyl alcohol	Kaplan, Burlinson, and Sitzmann (1975); Epstein, Sommer, and Hackley (1978)
3,5-dinitrophenol	Kaplan, Burlinson, and Sitzmann (1975); Epstein, Sommer, and Hackley (1978)
2,2'-dicarboxyl-3,3',5,5'-tetranitroazoxybenzene	Kaplan, Burlinson, and Sitzmann (1975)
2,4,6-trinitrobenzoic acid	Kaplan, Burlinson, and Sitzmann (1975)
N-(2- carboxy-3,5-dinitrophenyl)-2,4,6-trinitrobenzamide	Kaplan, Burlinson, and Sitzmann (1975)

4,6-dinitro-1,2-benzisoxazole	Epstein, Sommer, and Hackley (1978)